Spinodal of liquid water

Peter H. Poole,* Francesco Sciortino,† Ulrich Essmann,‡ and H. Eugene Stanley
Center for Polymer Studies and Physics Department, Boston University, Boston Massachusetts 02215
(Received 26 May 1993)

An open question in the study of water concerns the shape of the liquid spinodal line in the phase diagram of water, a boundary which represents the limit of mechanical stability of the liquid state. It has been conjectured that the pressure of the liquid spinodal $P_s(T)$ does not decrease monotonically with decreasing temperature T, but passes through a minimum and is "reentrant" from negative to positive pressure P in a region of T in which the liquid is deeply supercooled. The conjectured minimum in $P_s(T)$ has not been directly observed due to the difficulties encountered in experiments which attempt to study liquid water under tension. Here we exploit the ability of molecular-dynamics computer simulations to model the behavior of liquid water deep into its metastable region. We thereby attempt to observe a minimum in $P_s(T)$. We first argue that the ST2 potential of Stillinger and Rahman [J. Chem. Phys. **60**, 1545 (1974)] is the best of several commonly used water interaction potentials for this purpose. Then, we conduct simulations of a system of ST2 particles over a wide range of stable and metastable liquid-state points, and demonstrate that $P_s(T)$ for ST2 is not reentrant. In a second set of simulations we test if the behavior we find is limited to the ST2 potential by exploring the relevant thermodynamic region of the liquid as simulated by the TIP4P interaction potential of Jorgensen *et al.* [J. Chem. Phys. **79**, 926 (1983)]. We find that the TIP4P potential confirms the absence of a reentrant spinodal. We also show how the structural and energetic properties of both the ST2 and TIP4P liquids are consistent with the absence of a reentrant spinodal.

PACS number(s): 64.70.Fx, 64.30.+t, 61.20.Ja, 61.25.Em

I. INTRODUCTION

The liquid spinodal line is the limit of stability of the (metastable) liquid state with respect to fluctuations toward a thermodynamically stable phase, such as the gas. In normal liquids, the liquid spinodal line begins at the liquid-gas critical point and, in the plane of pressure P and temperature T, decreases monotonically with decreasing T along a path lying below the liquid-gas coexistence curve, as shown in Fig. 1(a).

It has been conjectured that such behavior is not observed in the case of liquid water. As first suggested by Speedy and Angell [1], and later developed by Speedy [2–4] into the "stability-limit conjecture" (SLC), the liquid spinodal line for water is "reentrant": it has a minimum at negative P and passes back to positive P as T decreases further, as shown in Fig. 1(b). The increasingly anomalous thermodynamic behavior of liquid water as it is cooled at positive P [5–7] can be interpreted in terms of the approach to such a reentrant spinodal [1–4,8,9]. For example, the maximum in the density ρ of water at 4 °C and the minimum in the isothermal compressibility K_T at 46 °C are possibly manifestations of spinodal-induced thermodynamic singularities occurring in the supercooled region. Thus the SLC suggests that the thermodynamic anomalies of liquid water arise from a single reentrant spinodal line that determines both the limit of liquid superheating at high T and of supercooling at low T.

The SLC is strongly related to the existence of a line in the P-T plane along which the density of liquid water is a maximum: the temperature of maximum density (TMD) line [10,11]. Indeed, for any liquid with a density maximum, it has been shown on the basis of thermodynamic arguments by Debenedetti and co-workers [12–16] that the most physically plausible way for the TMD line to terminate is at an intersection with a spinodal line. Furthermore, it is shown in Speedy's original statement of the SLC that an intersection in the P-T plane of a negatively sloped TMD line with a positively sloped liquid spinodal line requires that the liquid spinodal has a minimum at the intersection point [2]. Therefore, at T less than that of the intersection point, the spinodal is negatively sloped and will occur at higher P as T decreases. Since the intersection of the TMD and spinodal lines is in general expected to occur in the negative P region of the P-T plane, the possibility arises that the spinodal passes from negative to positive P as T decreases, as predicted by the SLC, and illustrated in Fig. 1(b).

The thermodynamic arguments used to arrive at the above conclusions can predict the behavior of the spinodal line close to specific points, such as its intersection with the TMD line. However, they do not give a good indication of the specific shape of the spinodal in the entire P-T plane. To overcome this problem, and also to understand the global thermodynamic features in terms of microscopic behavior, several simple models of liquids with a density maximum have been proposed and studied analytically in the last few years [16,17]. Part of this work has focused on the relation between the den-

*Present address: Department of Chemistry, Arizona State University, Tempe, AZ 85287.
†Present address: Dipartimento di Fisica, Università "La Sapienza," Piazzale Aldo Moro, 00185 Roma, Italy.
‡Present address: Department of Chemistry, University of North Carolina, Chapel Hill, NC 27599.

 ©1993 The American Physical Society

sity maximum line and the liquid spinodal. Such models have confirmed the general validity of the analysis of Speedy and of Debenedetti and co-workers concerning the behavior of the spinodal near its intersection with the TMD line, but have also made clear that possibilities consistent with the reentrance of the spinodal, but different from the SLC, are possible.

To study the scenario proposed by the SLC we have performed a comprehensive series of molecular-dynamics (MD) simulations, with an intermolecular potential commonly used to model liquid water. In contrast to experiments [11,18–20], where the challenges encountered in studies of liquid water under tension restrict the types of measurements that are possible, the MD technique allows a clear determination of both TMD and spinodal lines, in the positive as well as negative P regions of the phase diagram.

The MD study presented here, which extends and completes the data presented in a recent paper [21], suggests that the spinodal line in water is *not* reentrant. We show that the intersection of the TMD line and the spinodal is avoided by a change of slope of the TMD line itself. Such a change of slope, observed under tension, reflects the change in the liquid structure toward a random tetrahedral network configuration.

The paper is organized as follows: In the remainder of Sec. I we recall the definitions of metastability and of a spinodal, and then review the motivations and predictions of the SLC. We also review previous attempts to study the spinodal line in computer simulations of liquid

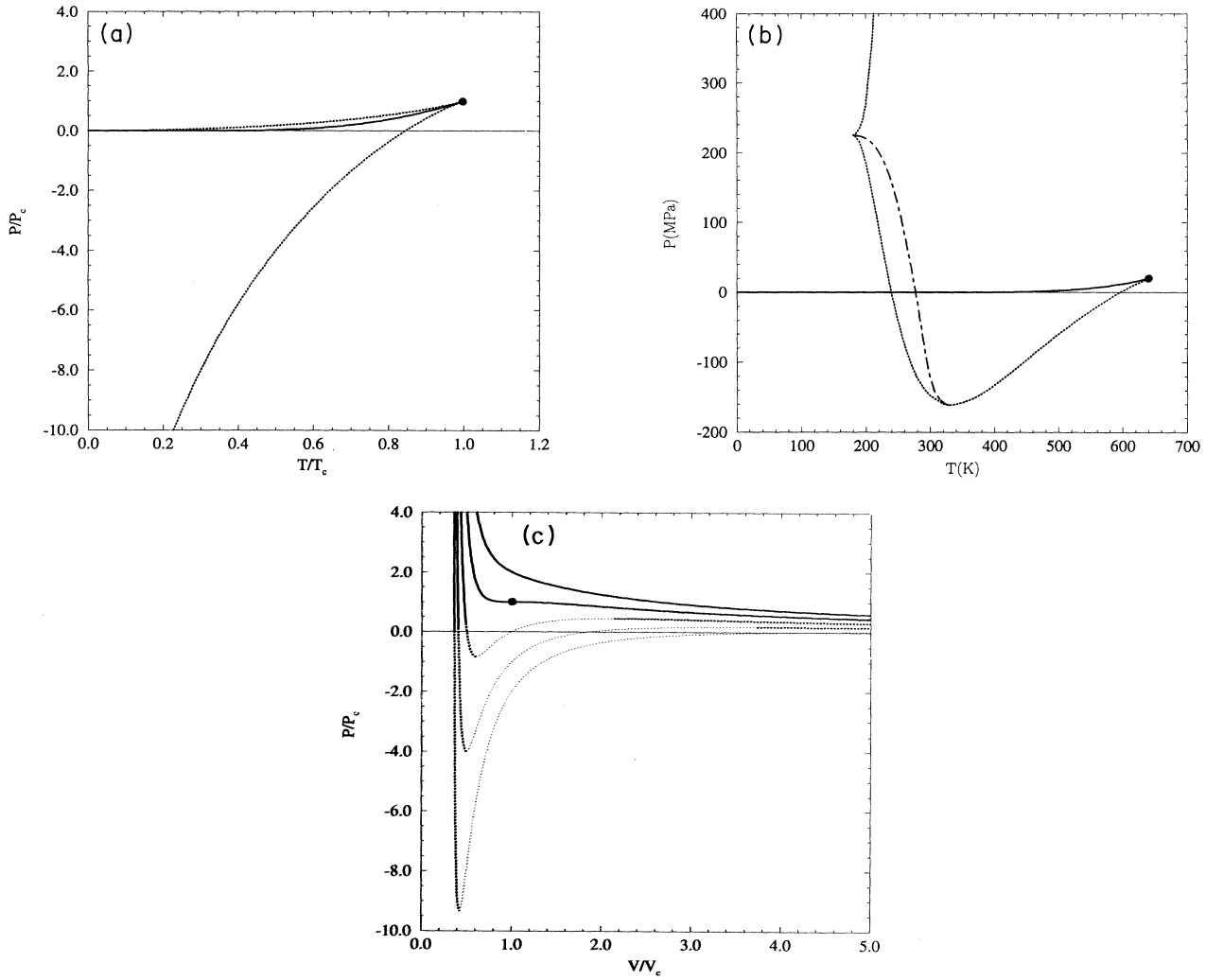

FIG. 1. (a) Phase diagram of the van der Waals fluid in the P-T plane. The liquid-gas coexistence line is shown as a solid line ending in the critical point (•). The gas and liquid spinodals are shown as dotted lines. (b) Phase diagram predicted by the SLC. The liquid-gas coexistence line (heavy line) ends in the critical point (•). The liquid spinodal (dotted line) bounds the entire superheating, stretching, and supercooling regimes, and becomes reentrant where it meets the TMD line (dot-dashed line) at negative P. (c) $P_T(V)$ isotherms of the van der Waals equation, above and below the critical temperature. Solid lines identify thermodynamically stable states, thick dotted lines metastable states, and thin dotted lines unstable states. The critical values of P, T, and V are denoted with the subscript c.

water. In Sec. II we show that, of several water interaction potentials, the ST2 potential of Stillinger and Rahman [22] is best suited to an exploration of the thermodynamic features whose properties are predicted in the SLC. In Sec. III we report a detailed study of the means by which the liquid spinodal and TMD line can be located from the ST2 simulation results, and further, that simulations using the TIP4P [23] potential of Jorgensen *et al.* confirm the ST2 behavior. In Sec. IV, the observed behavior of the TMD line is shown to be consistent with that of the spinodal, and is confirmed in simulations of larger ST2 systems. Again, the behavior of the TMD line as found in the ST2 simulations is confirmed in studies using the TIP4P potential. In Secs. V and VI, the energetic and structural properties of the liquid close to the spinodal are examined.

A. Metastability and spinodals

In the space of variables identifying the thermodynamic state of a system, the boundary between metastable and unstable states is the spinodal, the limit of metastability of the system [24]. The properties of the spinodal in a mean-field approach are simply illustrated by the classical van der Waals description of a liquid-gas system [25]. Figure 1(c) shows $P_T(V)$ isotherms of the pressure of the van der Waals equation as a function of the specific volume V for a number of T both above and below the critical temperature T_c. The negative inverse of K_T, defined through the relation

$$-K_T^{-1} \equiv V\left(\frac{\partial P}{\partial V}\right)_T, \tag{1.1}$$

is proportional to the slope of isotherms in Fig. 1(c). *Unstable* states are located on the portions of the isotherms where the slope is *positive*. States for which $K_T > 0$ are either thermodynamically stable or metastable, while states for which $K_T < 0$ are unstable. The points along each $P_T(V)$ isotherm at which the slope, and thus K_T, changes sign are the extrema of the van der Waals isotherms. Since metastable states occur between unstable and thermodynamically stable states, the isotherm extrema identify the limit of the region of metastable states, which is the spinodal.

The P-T phase diagram of the van der Waals fluid, shown in Fig. 1(a), is the projection into the plane of P and T of the line of coexistence between liquid and gas, which terminates in the critical point C. Also shown are the projections onto the P-T plane of the spinodals. One, the "gas spinodal," lies above the liquid-gas coexistence line. Between this upper spinodal and the coexistence line, the gas phase may be observed as a metastable state since the liquid phase is the thermodynamically stable phase everywhere above the coexistence line. This gas spinodal thus indicates the maximum extent to which a gaseous state may penetrate the stable liquid region of the phase diagram before condensing into the liquid state.

Below the coexistence line lies another spinodal, the "liquid spinodal." Between the liquid spinodal and the coexistence line, the liquid phase may be observed as a metastable state. Note that the liquid spinodal extends into the region of *negative* P. This expresses the fact that the liquid spinodal, at low T, indicates the maximum tensile stress to which the homogeneous liquid may be subjected before cavitating. Although the liquid spinodal and the gas spinodal are related through their common end point C, we only consider here the properties of the liquid spinodal. Hence, in what follows, "spinodal" is meant to refer specifically to the *liquid* spinodal.

The mean-field behavior displayed by the van der Waals equation in Fig. 1(c) shows that the spinodal represents a thermodynamic singularity. For example, from Eq. (1.1), it can be seen that K_T diverges to infinity at the spinodal, in a manner qualitatively similar to the K_T divergence predicted at the critical point C. Thus the mean-field spinodal may be regarded as a line of "pseudocritical" points [26].

B. The stability limit conjecture

Many static and dynamic properties of liquid water exhibit strong and anomalous deviations from those expected of a simple liquid. For example, response functions like K_T [1] and the isobaric specific heat C_P [27] are observed to increase rapidly as the temperature of the liquid decreases, especially in the T range in which the liquid is supercooled. The SLC was motivated by the observation that the rapid changes observed in many such properties X of water as it is cooled appear to display the diverging power-law form

$$X = A_X \epsilon^{-\lambda_X}, \tag{1.2}$$

where $\epsilon \equiv (T - T_s)/T_s$, with T_s being the temperature of singularity, and A_X and λ_X are respectively the amplitude and exponent associated with the divergence of the quantity X. At atmospheric P, experimental data have been fit to the form in Eq. (1.2) for $X = K_T$, ρ, the isobaric expansivity α_P, the shear viscosity, the dielectric relaxation time [1], the diffusion constant [1,8,9], and various nuclear spin relaxation times [1,6]. For all these quantities, T_s appears to be close to 228 K$= -45$ C [28].

Fits of isobars of K_T to Eq. (1.2) at different P up to 190 MPa indicate that T_s shifts to lower T at higher P [29]. Furthermore, T_s is found deep in the region of the phase diagram where the liquid is metastable with respect to the formation of crystalline ice, and seems to remain a constant 5 to 15 K below the lowest T to which liquid water has been successfully supercooled, the homogeneous nucleation limit T_H [30]. This suggests that the line formed by the values of T_s at different P represents a boundary in the phase diagram of the liquid beyond which the liquid cannot exist, not even as a metastable state. The increasing magnitudes of response functions observed on approach to this T_s line indicate increasingly large density fluctuations which ultimately prompt nucleation of the ice phase before the T_s line is reached. Given that the T_s line therefore both delimits the end of the re-

gion of metastable liquid states, and also locates a line of thermodynamic divergences, the T_s line was identified in the SLC with a spinodal line.

As mentioned in Sec. I, Speedy showed [2] that the appearance of an unexpected spinodal in the phase diagram of water is perhaps not surprising given the presence and shape of the TMD line in the phase diagram. The temperature 4 C is the point on the TMD line corresponding to atmospheric P. For P greater than atmospheric P, the TMD occurs at $T < 4$ C, and so the TMD line is negatively sloped in the P-T plane for $P > 0$ [10]. On the TMD line, V is an extremum with respect to T since α_P, defined by

$$\alpha_P \equiv (1/V)\left(\frac{\partial V}{\partial T}\right)_P, \tag{1.3}$$

is zero. Note that since $\alpha_P = 0$ on the TMD line, then the thermal pressure coefficient γ_V, defined by

$$\gamma_V \equiv \left(\frac{\partial P}{\partial T}\right)_V, \tag{1.4}$$

is also zero, because of the thermodynamic identity,

$$\gamma_V = \alpha_P / K_T. \tag{1.5}$$

As a consequence, a point on the TMD line can also be located as a minimum in $P_\rho(T)$, an isochore of P as a function of T.

As summarized in Appendix A, the behavior of the TMD line may be associated with a change of direction in the spinodal line. Thereby follows an important prediction of the SLC: The TMD line intersects the liquid spinodal originating at the liquid-gas critical point. This intersection, in the metastable liquid under tension (i.e., at $P < 0$) requires a spinodal minimum to occur, followed at lower T by the reappearance of the spinodal at positive P in the region of the phase diagram where the liquid is supercooled. This is the reentrant spinodal having the form shown in Fig. 1(b).

C. Computer simulations

The intersection of the spinodal and the TMD line is predicted by the SLC to occur in a region of negative P which is experimentally difficult to probe because of nucleation of the gas phase within the metastable liquid under tension. In general, nucleation of the stable phase always prevents the experimental study of states arbitrarily close to a spinodal line [20,24]. In the present work, we exploit the ability of computer simulations to study metastable liquid states. Computer simulations of systems containing one species of particle and which use periodic boundary conditions necessarily do not incorporate the impurities or surfaces which trigger the heterogeneous nucleation of the stable phase observed in experiments. Also, the metastable liquid can usually be simulated for a time which is long enough for the evaluation of thermodynamic properties, but which is shorter than the characteristic time for homogeneous nucleation of the stable phase.

Previous attempts have been made to confirm or refute the SLC using computer simulations. Okasaki, Kataoka, and co-workers [31–35] studied the properties of several water models for the purpose of assessing their ability to reproduce the thermodynamic anomalies of water. In all cases, their strategy was to simulate hundreds of thermodynamic states. Their resulting data were fit to a multinomial equation of state (EOS), from which thermodynamic properties were calculated. Although the direct determination of the shape of the spinodal line was not the principal focus of these works, an *extrapolation* of their EOS predicted that the liquid spinodal was reentrant from negative to positive pressure at supercooled temperatures.

Recently, Striemann [36] studied a system of particles interacting through the ST2 water interaction potential for the purpose of attempting to directly observe the effects produced by the reentrant liquid spinodal at low temperature. In this study, the simulated liquid was examined for evidence that an instability would be encountered if the liquid was cooled isobarically at a number of different P. No sign of a low temperature instability was found in this study, suggesting that the spinodal is not reentrant.

Given the conflicting conclusions of these earlier works, and the lack of a clear determination of the relation between the TMD line and the liquid spinodal, we attempt here a direct and comprehensive study of the liquid behavior at negative P. Our principal aim is to determine the position and shape of the spinodal and the TMD lines of simulated liquid water, in order to gauge the extent to which the predictions of the SLC are borne out.

II. CHOICE OF INTERPARTICLE POTENTIAL

There are many interparticle potentials commonly used to simulate liquid water. The SLC predicts that the liquid spinodal is reentrant in the P-T phase diagram at temperatures below those of the TMD line; see Fig. 1(b). Our interparticle potential must give rise to a simulated liquid that (1) exhibits a TMD line, and (2) allows equilibrium simulations to be carried out at temperatures below those at which the TMD line is observed. We therefore conduct a preliminary simulation study on several water pair potentials to determine the extent to which these two criteria are satisfied by each. Specifically, the ST2 and TIP4 potentials as well as the SPC/E [37] potentials of Berendsen *et al.*, are chosen as candidates, as each of these has been extensively used for simulation studies of bulk water [38].

Each of these three potentials is simulated at $\rho = 1.0$ g/cm^3 at a number of temperatures. (A summary of the simulation method used is given in Appendix B.) The average P for each T is calculated and the resulting isochore of $P_\rho(T)$ for each potential is plotted in Fig. 2. At the lowest temperatures simulated, in the region near $T = 200$ K, the molecular mobility is becoming increasingly low. The simulated systems thus become increasingly difficult to equilibrate, and so the given isochores do not extend beyond this region. The success of each potential in reproducing the experimental P, and its T

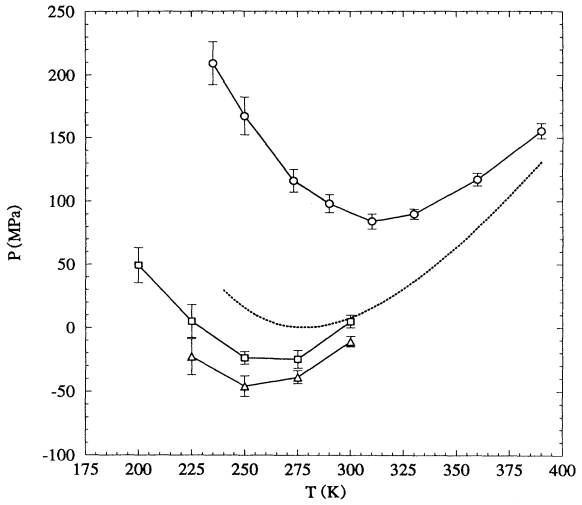

FIG. 2. $\rho = 1.0$ g/cm^3 isochores of $P_\rho(T)$ for three water pair potentials, ST2 (○), TIP4P (□), and SPC/E (△), compared with the experimental $P_\rho(T)$ isochore (dotted line) as reproduced by the Haar-Gallagher-Kell equation of state [39], at the same density.

dependence, is assessed by comparing the simulated isochores with the experimental $P_\rho(T)$ isochore of water at $\rho = 1.0$ g/cm^3 [39], also shown in Fig. 2.

As noted in Sec. I B, the temperature at which a minimum in $P_\rho(T)$ occurs identifies a TMD. Both TIP4P and SPC/E give $P_\rho(T)$ minimum in the vicinity of 260 K, which is approximately 17 K below the experimental TMD for the $\rho = 1.0$ g/cm^3 isochore. This lowering of the TMD at $\rho = 1.0$ g/cm^3 in TIP4P and SPC/E suggests that the thermodynamic anomalies of these simulated liquids are somewhat weaker than in real water. Nevertheless, both of these pair potentials provide the opportunity to study the anomalous region of the liquid up to 60 K below the TMD.

The ST2 potential exhibits a TMD approximately 35 K *above* the experimental TMD, and so allows equilibrium simulations of states up to 80 K below its TMD. Such behavior is consistent with what is known about how well ST2 reproduces other properties of liquid water. For example, there is evidence that the melting temperature of ST2 may also be elevated over that of real water [40]. In principle, ST2 overemphasizes the tetrahedral character of the H–bonding groups on the water molecule since both donor protons and acceptor lone-pair electrons are modeled as explicit force centers. As the tendency to form tetrahedral molecular arrangements is closely associated with the appearance of macroscopic anomalies in water, the anomalies of the ST2 liquid are expected to be correspondingly stronger than in real water, and will appear at higher temperature [38]. In the present context, the deviations of the properties of the ST2 model from those of real water are an advantage, since they facilitate the simulation of states at the lowest temperatures relative to the TMD. Thus ST2 can be used to probe most deeply the thermodynamic properties and structure of the system in the region both where the liquid is strongly anomalous, and where the reentrant spinodal is predicted to be found. For this reason, most of the simulations carried out for this study are devoted to the study of a system of ST2 particles.

However, there exists the danger that the quantitative differences between ST2 properties and those of real water induce a qualitatively different phase behavior from the point of view of locating the limits of stability of the liquid. This concern suggests that the behavior seen in ST2 should be confirmed, at least in its critical aspects, in simulations using the TIP4P or SPC/E potentials, since they too allow for a study of the anomalous region below the TMD.

A summary of 62 states simulated with the ST2 potential, and 32 states simulated with the TIP4P potential, is given in Tables II, III and IV. Presented are the values of ρ and T selected for each simulation, the length of each run, and the values of P and the internal potential energy U that resulted. For some states, the diffusion constant D is also given.

III. THE SPINODAL LINE

In this section, we first systematically explore several distinct approaches to calculate the position of the spinodal in the ST2 simulations. Then the results are shown to be consistent with the behavior found in the TIP4P simulations.

A. Minima in $P_T(\rho)$ isotherms

As noted in Sec. I A, the liquid spinodal occurs at the minimum of an isotherm of P versus V, and hence, equivalently at the minimum of an isotherm of P versus ρ. The behavior of the $P_T(\rho)$ isotherms from the ST2 data can therefore be examined to give an estimate of the location in the phase diagram at which the spinodal of the liquid state under tension may be found. Figure 3(a) shows the five $P_T(\rho)$ isotherms from the ST2 liquid-state data given in Tables II and III that exhibit such a minimum [41]. As ρ decreases, $P_T(\rho)$ decreases more and more slowly and exhibits a minimum at the smallest values of ρ. This behavior is similar to that expected of $P_T(\rho)$ as the mean-field spinodal is approached. The lowest value of P found along each $P_T(\rho)$ isotherm is thus taken as an estimate of $P_s(T)$.

The resulting estimate for the spinodal line $P_s(T)$ is plotted in Fig. 3(b). Also shown are $P_\rho(T)$ isochores, obtained by constructing a bicubic spline model [42] of the data set in Tables II and III. The line connecting the estimated $P_\rho(T)$ isochore minima for different ρ locates the TMD line. Notably, the TMD line avoids the spinodal line, by changing slope in the negative pressure region. The spinodal $P_s(T)$ continues to decrease as T decreases, *even in the temperature region where a TMD is observed.* This behavior (which we discuss in more detail in Sec. IV) is qualitatively different from that predicted by the SLC.

B. Power-law behavior of $P_T(\rho)$ isotherms

In this section, we obtain an independent set of estimates of $P_s(T)$ by fitting the data to the anticipated power-law relationship between P and ρ near the spin-

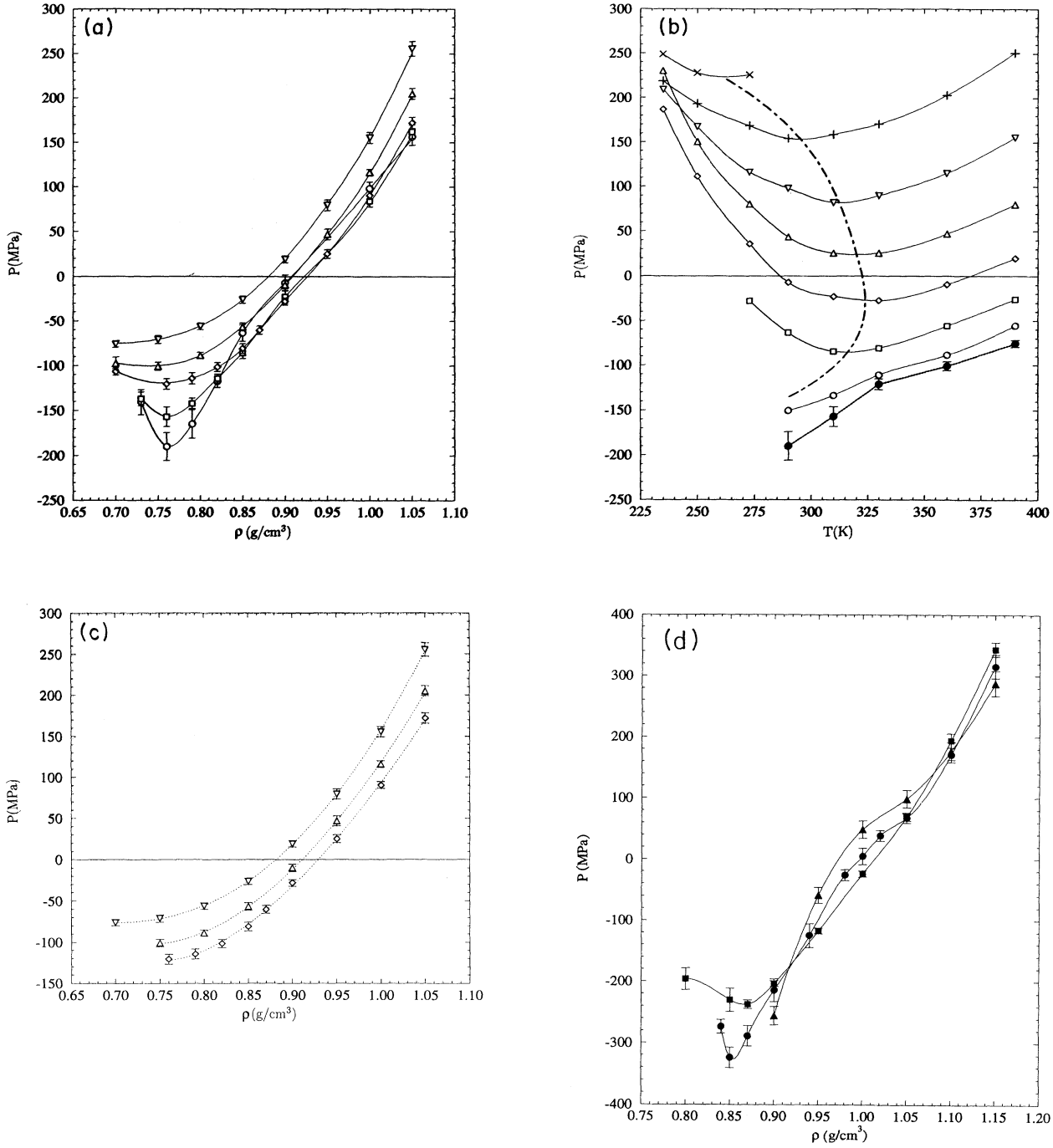

FIG. 3. (a) $P_T(\rho)$ isotherms for the ST2 liquid, for $T = 390$ K ($\bigtriangledown$), $T = 360$ K ($\bigtriangleup$), $T = 330$ K ($\diamond$), $T = 310$ K ($\square$), and $T = 290$ K ($\circ$). Splines (solid lines) are drawn through each isotherm. The spinodal values $P_s(T)$ are estimated from the minima at each temperature: $P_s(390\text{ K}) = -76 \pm 4$ MPa, $P_s(360\text{ K}) = -101 \pm 5$ MPa, $P_s(330\text{ K}) = -121 \pm 6$ MPa, $P_s(310\text{ K}) = -157 \pm 11$ MPa, and $P_s(290\text{ K}) = -190 \pm 16$ MPa. (b) $P_\rho(T)$ isochores for the ST2 liquid, for $\rho = 1.10$ g/cm^3 ($\times$), $\rho = 1.05$ g/cm^3 ($+$), $\rho = 1.00$ g/cm^3 ($\bigtriangledown$), $\rho = 0.95$ g/cm^3 ($\bigtriangleup$), $\rho = 0.90$ g/cm^3 ($\diamond$), $\rho = 0.85$ g/cm^3 ($\square$), and $\rho = 0.80$ g/cm^3 ($\circ$). The isochores are obtained by constructing a bicubic spline model of the data set in Tables II and III. The estimate for the spinodal, $P_s(T)$, based on the value of P at the minima of the isotherms in (a), is given by the filled dots and dotted line. The TMD line (dot-dashed line) is also plotted. (c) $P_T(\rho)$ ST2 isotherms fitted to Eq. (3.1), for $T = 390$ K ($\bigtriangledown$), $T = 360$ K ($\bigtriangleup$), and $T = 330$ K ($\diamond$). The dotted lines are the fitted curves, for which the fit parameters are given in Table I. (d) $P_T(\rho)$ isotherms for the TIP4P liquid, for $T = 250$ K (filled $\square$), $T = 225$ K (filled $\circ$), and $T = 200$ K (filled $\bigtriangleup$). Splines (solid lines) are drawn through each iostherm.

TABLE I. Fits of $P_T(\rho)$ isotherms to Eq. (3.1)

T (K)	P_s (MPa)	ρ_s (g/cm^3)	δ	A (cm$^{3\delta}$MPa/g$^\delta$)
390	-76 ± 4	0.70 ± 0.04	2.3 ± 0.3	3500 ± 500
360	-101 ± 6	0.74 ± 0.03	1.8 ± 0.3	2600 ± 400
330	-121 ± 6	0.76 ± 0.02	1.6 ± 0.2	2200 ± 300

odal. The virtue of this independent set of estimates is that it utilizes the data at densities away from the density which gives rise to a minimum in the $P_T(\rho)$ isotherms of Fig. 3(a). Specifically, in Fig. 3(c) we fit all the data for the $T = 390$ K, 360 K, and 330 K isotherms to a power law of the form

$$P - P_s(T) = A[\rho - \rho_s(T)]^\delta, \tag{3.1}$$

where A is a constant, δ is the critical exponent characterizing the shape of isotherms in the spinodal region, and $\rho_s(T)$ is the density of the spinodal at temperature T [25,26]. The values that result for the fitted parameters are shown in Table I.

The success of this fitting for these values of T, shown in Fig. 3(c), confirms that spinodal-like behavior can be observed over a range of states, and not only at the stability limit itself. Fitting the data to Eq. (3.1) is particularly useful because it exploits data describing states away from the spinodal, where finite-size effects due to the size of the simulated system are likely to be less important since the correlation length is reduced from its value near the spinodal. The fact that Table I shows the same values of $P_s(T)$ and $\rho_s(T)$ that may be estimated from the $P_T(\rho)$ minima in Fig. 3(c) indicates that even close to the instability, finite-size and nucleation effects are not perturbing the results enough to mask the thermodynamic manifestation of spinodal behavior. Finally, note that the value of δ found is close to the value $\delta = 2$ predicted in mean–field theory for the spinodal [26].

The $T = 310$ K and $T = 290$ K $P_T(\rho)$ isotherms of Fig. 3(a) are not fit to Eq. (3.1) because of the strong deviations from a simple power law that appear along these isotherms at densities above that of their minima. In particular, this deviation involves a change in the sign of the curvature of the $P_T(\rho)$ isotherms, a behavior not previously predicted to occur in liquid water. This unexpected feature (also observed in the TIP4P data — see Sec. III D) can, however, be shown to be consistent with the known thermodynamic properties of liquid water, as shown in detail elsewhere [21,43].

C. Mechanical stability of simulated states

If the spinodal $P_s(T)$ of the ST2 liquid is located as indicated in Fig. 3(b), then those metastable states for

TABLE II. The ST2 data set at low T: constant-V simulations of $N = 216$ molecules, where T is maintained near the specified values using Berendsen's method with $\tau_T = 0.5$ ps. Most of these runs were carried out on workstations requiring approximately 1 CPU day of computation for each 80 ps of simulation.

T (K)	ρ (g/cm^3)	$P \pm \delta P$ (MPa)	$U \pm \delta U$ (kJ/mol)	D (10^{-5}cm^2/s)	t_f (ps)
235	1.10	249 ± 15	-46.12 ± 0.08	0.34	636
235	1.05	218 ± 12	-46.78 ± 0.16		615
235	1.00	209 ± 27	-47.39 ± 0.13	0.18	799
235	0.95	230 ± 31	-48.48 ± 0.12		934
235	0.92	209 ± 17	-48.97 ± 0.10		1354
250	1.10	228 ± 12	-45.10 ± 0.08	0.57	652
250	1.05	193 ± 10	-45.54 ± 0.08	0.50	696
250	1.00	167 ± 15	-46.07 ± 0.11		833
250	0.95	150 ± 12	-46.99 ± 0.13	0.17	755
250	0.92	131 ± 24	-47.53 ± 0.22	0.10	793
250	0.87	75 ± 17	-48.48 ± 0.11	0.003	725
273	1.10	227 ± 10	-43.45 ± 0.08	1.36	391
273	1.05	168 ± 12	-43.62 ± 0.10	1.00	358
273	1.00	116 ± 9	-44.10 ± 0.07	0.96	735
273	0.95	80 ± 7	-44.72 ± 0.15	0.63	561
273	0.90	35 ± 11	-45.62 ± 0.10	0.32	546
273	0.87	-2 ± 10	-46.21 ± 0.16		642
273	0.85	-28 ± 11	-46.79 ± 0.16	0.16	807
273	0.84	-52 ± 17	-47.50 ± 0.22		398
290	1.05	156 ± 9	-42.44 ± 0.07	1.87	365
290	1.00	98 ± 7	-42.56 ± 0.13	1.75	253
290	0.90	-7 ± 9	-43.59 ± 0.29	1.17	560
290	0.85	-64 ± 9	-44.65 ± 0.34		754
290	0.82	-118 ± 7	-44.34 ± 0.25	0.63	500
290	0.79	-165 ± 16	-44.41 ± 0.09		827
290	0.76	-190 ± 16	-43.70 ± 0.44	0.57	458
290	0.73	-141 ± 14	-42.50 ± 0.25		189
290	0.70	-128 ± 15	-42.32 ± 0.26		139

which $P > P_s(T)$ and $\rho > \rho_s(T)$, while perhaps not thermodynamically stable, are mechanically stable, while any state not satisfying these two conditions will be unstable. In this section, we shall check the stability of the states in Tables II and III, to provide an independent confirmation of the estimates for $P_s(T)$ reported in Fig. 3(b). This stability check is also important because thus far we have not confirmed that the system is indeed mechanically stable up to the spinodal limits reported.

A simulated liquid can be tested in a particularly striking way for the presence or absence of mechanical stability by simulating the system using an algorithm which constrains P, rather than V as in the simulations described thus far. With P constrained, V must take on that value which satisfies the condition of mechanical stability.

We distinguish two cases

(i) Attempts to simulate liquid states at a pressure value $P < P_s(T)$ should fail since no liquid states are possible at such P for any value of ρ. Such a simulated system, its tensile limit exceeded, should be observed to "cavitate" to a gaslike phase containing large voids. Therefore we use constant-P continuations of the constant-V simulations to confirm the existence of a tensile limit at $P_s(T)$ [44]. Specifically, we find the constant-P continuation of the simulation at ($T = 330$ K, $\rho = 0.76$ g/cm^3), with fixed $P = -115$ MPa, and of that at ($T = 290$ K, $\rho = 0.76$ g/cm^3), with fixed $P = -180$ MPa, to be stable over 200 ps of continued simulation. However, constant-P continuations of the same simulations using fixed $P = -127$ MPa and $P = -193$ MPa, respectively, cavitate after a few tens of picoseconds of continued simulation. This test places bounds on the region of P over which the liquid state loses mechanical stability at $T = 330$ K and 290 K. The bounds we find bracket the estimates of $P_s(T)$ shown in Fig. 3(b).

(ii) Conversely, attempts to simulate liquid states at a pressure $P > P_s(T)$ with $\rho < \rho_s(T)$ should also fail: the density of the system should either *increase* [to give the stable liquidlike density above $\rho_s(T)$], or catastrophically *decrease* [in the direction to give the stable gaslike density far below $\rho_s(T)$]. Therefore, to confirm that the spinodal is near the points indicated in Fig. 3(b), the system trajectories resulting from the constant-V simulations conducted near the $P_T(\rho)$ minima are continued in constant-P simulations. We find that those states hav-

TABLE III. The ST2 data set at high T: constant-V simulations of $N = 216$ molecules, where T is maintained near the specified values using Berendsen's method with $\tau_T = 0.5$ ps.

T (K)	ρ (g/cm^3)	$P \pm \delta P$ (MPa)	$U \pm \delta U$ (kJ/mol)	D (10^{-5} cm^2/s)	t_f (ps)
310	1.05	162 ± 8	-41.01 ± 0.06		216
310	1.00	84 ± 6	-41.07 ± 0.07		346
310	0.90	-23 ± 7	-41.42 ± 0.21		213
310	0.85	-86 ± 6	-41.73 ± 0.14		294
310	0.82	-114 ± 5	-41.51 ± 0.13		545
310	0.79	-142 ± 6	-41.24 ± 0.27		320
310	0.76	-157 ± 11	-40.69 ± 0.14		647
310	0.73	-137 ± 8	-40.33 ± 0.14		332
330	1.05	172 ± 6	-39.69 ± 0.08		425
330	1.00	90 ± 4	-39.69 ± 0.04		590
330	0.95	25 ± 5	-39.60 ± 0.07		466
330	0.90	-28 ± 4	-39.56 ± 0.07		480
330	0.87	-60 ± 5	-39.44 ± 0.09	3.62	471
330	0.85	-81 ± 5	-39.41 ± 0.15	4.48	384
330	0.82	-102 ± 5	-39.23 ± 0.14	3.92	257
330	0.79	-114 ± 6	-38.70 ± 0.13	3.85	240
330	0.76	-121 ± 6	-38.38 ± 0.15	3.76	505
330	0.70	-107 ± 4	-37.63 ± 0.09	5.22	569
360	1.05	205 ± 6	-38.00 ± 0.05		283
360	1.00	117 ± 5	-37.76 ± 0.05		259
360	0.95	47 ± 6	-37.51 ± 0.07		298
360	0.90	-10 ± 4	-37.27 ± 0.07		334
360	0.85	-57 ± 4	-36.73 ± 0.08		358
360	0.80	-89 ± 4	-36.22 ± 0.07		400
360	0.75	-101 ± 5	-35.60 ± 0.07		414
360	0.70	-98 ± 7	-34.93 ± 0.06		270
390	1.05	255 ± 8	-36.50 ± 0.05		134
390	1.00	155 ± 6	-36.10 ± 0.05		236
390	0.95	79 ± 6	-35.74 ± 0.05		189
390	0.90	19 ± 4	-35.26 ± 0.04		443
390	0.85	-26 ± 4	-34.77 ± 0.05		301
390	0.80	-56 ± 4	-34.13 ± 0.06		344
390	0.75	-71 ± 4	-33.46 ± 0.05		278
390	0.70	-76 ± 4	-32.82 ± 0.07		193

ing $\rho > \rho_s(T)$ do not exhibit a change in density during the constant-P simulations, indicating stability. However, those states having $\rho < \rho_s(T)$ display behavior in which their density either increases [shifting these states to the stable liquid side of the $P_T(\rho)$ isotherm minimum], or decreases enormously (shifting the system to a stable gaslike state).

D. Confirmation in the TIP4P liquid

The TIP4P potential also exhibits a TMD, and so it is useful to compare the accompanying spinodal behavior to that found in the ST2 simulations. In analogy to the method of Sec. III A, the results of the TIP4P simulations given in Table IV are plotted in the form of $P_T(\rho)$ isotherms, shown in Fig. 3(d). Examination of the minima of the $P_T(\rho)$ isotherms shows that $P_s(T)$ at $T = 225$ K is *less than* $P_s(T)$ at $T = 250$ K. In Fig. 2 it was shown that a TMD occurs in the TIP4P simulations near $T = 260$ K. Therefore in TIP4P, like in ST2, $P_s(T)$ continues to decrease as T decreases even at temperatures below those at which a TMD is found. The overall shape of the family of $P_T(\rho)$ isotherms found using TIP4P is similar to that found using ST2, including the appearance of a change in the sign of the curvature of the $P_T(\rho)$ isotherms at the lowest T. The thermodynamic behavior of liquid water as simulated using the TIP4P potential is therefore consistent with the ST2 results: both potentials give behavior which is qualitatively different from that predicted by the SLC.

TABLE IV. The TIP4P data set: constant-V simulations of $N = 216$ molecules, where T is maintained near the specified values using Berendsen's method with $\tau_T = 0.5$ ps. Simulations for which $\delta t = 2$ fs rather than 1 fs are indicated with an *.

T (K)	ρ (g/cm^3)	$P \pm \delta P$ (MPa)	$U \pm \delta U$ (kJ/mol)	t_f (ps)
200	0.90	-256 ± 15	-48.96 ± 0.04	*5756
200	0.95	-59 ± 13	-49.23 ± 0.06	*3399
200	1.00	49 ± 14	-48.92 ± 0.14	*4585
200	1.05	99 ± 14	-48.63 ± 0.07	*2846
200	1.10	177 ± 15	-48.27 ± 0.10	*3912
200	1.15	288 ± 20	-48.29 ± 0.07	*1425
200	1.20	437 ± 13	-48.04 ± 0.08	*2299
225	0.84	-274 ± 11	-46.08 ± 0.22	294
225	0.85	-324 ± 17	-46.72 ± 0.15	839
225	0.87	-289 ± 17	-47.19 ± 0.22	2762
225	0.90	-215 ± 19	-47.38 ± 0.12	2217
225	0.94	-125 ± 19	-47.34 ± 0.16	2510
225	0.98	-26 ± 9	-47.17 ± 0.08	1970
225	1.00	5 ± 13	-47.19 ± 0.10	698
225	1.02	38 ± 9	-46.89 ± 0.08	992
225	1.05	68 ± 8	-46.81 ± 0.11	877
225	1.10	170 ± 12	-46.59 ± 0.06	*952
225	1.15	315 ± 19	-46.66 ± 0.05	*708
225	1.20	461 ± 12	-46.59 ± 0.09	*891
225	1.25	692 ± 11	-46.53 ± 0.10	*1239
225	1.30	954 ± 12	-46.55 ± 0.07	*1189
250	0.80	-196 ± 18	-43.76 ± 0.14	659
250	0.85	-230 ± 19	-44.12 ± 0.15	663
250	0.87	-237 ± 7	-44.49 ± 0.17	766
250	0.90	-204 ± 5	-44.93 ± 0.06	1794
250	0.95	-117 ± 5	-45.12 ± 0.07	*2000
250	1.00	-25 ± 5	-45.08 ± 0.04	1062
250	1.05	69 ± 6	-45.08 ± 0.06	*1158
250	1.10	194 ± 12	-45.08 ± 0.04	*1448
250	1.15	343 ± 12	-45.05 ± 0.05	*511
275	1.00	-25 ± 7	-43.33 ± 0.08	489
300	1.00	5 ± 5	-41.73 ± 0.05	367

IV. THE TMD LINE

The above data demonstrate that in the ST2 system the spinodal line $P_s(T)$ is not reentrant, even at temperatures below those at which a TMD is observed. Indeed, a spinodal is expected to become reentrant at the point where it interacts with the TMD line in the phase diagram (see Appendix A). The SLC is implicitly based on the assumption that the P-T projection of the TMD line always has negative slope. As indicated in Fig. 3(b), the TMD line has negative slope at positive and low negative pressures, but has positive slope at the largest negative pressures. This behavior of the TMD line prevents an intersection with the spinodal, in the range of T simulated. Furthermore, as discussed in Appendix A, a positively sloped TMD line cannot meet a positively sloped spinodal in a thermodynamically consistent phase diagram. Thus the TMD and the spinodal cannot meet in a region of T and P not probed in the simulations (unless the TMD line were to again change slope). Note that the appearance of a TMD line with positive slope is thermodynamically possible, and has been observed in simulations of a simple pair potential unrelated to ST2 or TIP4P, the Gaussian core model [45].

The importance of these considerations is that they show that the behavior of the TMD line in the ST2 liquid is in itself sufficient to demonstrate that the behavior of this simulated liquid is not consistent with the SLC. Though finite-size and boundary condition effects may skew the results from simulations of states near the spinodal, it is less likely that these problems extend into the region of states where the TMD line changes slope because the correlation lengths are smaller away from the spinodal. Thus we see that the conclusion that the ST2 liquid is inconsistent with the SLC can be based not only on the behavior of the spinodal line $P_s(T)$, but also on the overall thermodynamic properties of the stretched liquid.

A. Confirmation in larger ST2 systems

Ideally, in order to check for finite-size effects in our results, we should reproduce the isotherms used to locate the spinodal in a simulation of a much larger system. Unfortunately, the equilibration times in the present size system are already quite long, so simulations for a larger system would be computationally prohibitive. However,

since the appearance of a TMD line with positive slope is alone sufficient to prove an incompatibility between the ST2 liquid behavior and the SLC, the opportunity for a simpler check presents itself.

The $\rho = 0.80$ g/cm^3 $P_\rho(T)$ isochore in Fig. 3(b) is useful for demonstrating that the TMD line has positive slope because this isochore has no identifiable minima over a range of T for which isochores at higher P do have minima. If the only reason the TMD-spinodal line intersection is not observed in Fig. 3(b) is due to the finite size of the system studied, then this $\rho = 0.80$ g/cm^3 isochore must have a quite different shape in the limit of an infinitely large system—it must either display a minimum not seen in the $N = 216$ particle simulations, or it is not a metastable isochore at all (actually lying beyond the spinodal of the infinite system).

We therefore check the position and stability of points on the $\rho = 0.80$ g/cm^3 $P_\rho(T)$ isochore in a system containing $N = 1728$ particles. We perform a set of three constant-P simulations at $T = 290$ K, 330 K and 360 K [46]. The states simulated are $(N = 1728, P = -150$ MPa$, T = 290$ K$)$, $(N = 1728, P = -100$ MPa$, T = 330$ K$)$ and $(N = 1728, P = -80$ MPa$, T = 360$ K$)$. By allowing ρ to vary, the absolute stability of these states in the $N = 1728$ system is checked in the same way as described in Sec. III C.

We find that after 70 ps each of constant-P simulation, both the $T = 330$ K and $T = 360$ K simulations appear to be well past the equilibration stage and show no signs of cavitating. At $T = 330$ K, we found the density to be $\rho = 0.825 \pm 0.005$ g/cm^3 and $U = -39.3 \pm 0.3$ kJ/mol, while at $T = 360$ K, we found the density to be $\rho = 0.807 \pm 0.005$ g/cm^3 and $U = -36.4 \pm 0.2$ kJ/mol. As it is especially important to confirm the behavior of the $T = 290$ K system at $\rho = 0.80$ g/cm^3, it was evolved for 330 ps; we found $\rho = 0.797 \pm 0.005$ g/cm^3 and $U = -44.2 \pm 0.3$ kJ/mol, with no indications of cavitation.

The average values of ρ and U produced in each of these $N = 1728$ simulations are very close to being within error of what would be predicted from the data set of the $N = 216$ simulations; see Fig. 4. There does not therefore seem to be a large finite-size effect in these quantities when N is varied from 216 to 1728, confirming the phase behavior shown in Fig. 3(b).

B. Confirmation in the TIP4P liquid

Next we check if the results for the TMD line reported for the ST2 potential are valid for the TIP4P potential. In the same spirit as the checks described in Sec. IV A, we focus our tests on the question of whether the TIP4P potential *also* exhibits a TMD line which assumes a positive slope in the P-T plane, thus avoiding an intersection with the spinodal. As seen in Fig. 2, the TIP4P potential exhibits a minimum in the $\rho = 1.0$ g/cm^3 $P_\rho(T)$ isochore, demonstrating that the TMD line of TIP4P passes through this isochore at negative P near $T = 260$ K. The slope of the TMD line can be established in this region of the phase diagram by plotting the $\rho = 0.9$ g/cm^3 $P_\rho(T)$ isochore. A negatively sloped TMD line requires that the minimum of the $\rho = 0.9$ g/cm^3 $P_\rho(T)$ isochore occurs at a *higher* temperature than the minimum of the $\rho = 1.0$ g/cm^3 $P_\rho(T)$ isochore. The opposite behavior is associated with a positively sloped TMD.

Accordingly, in Fig. 5, we plot the $\rho = 0.9$ g/cm^3 and $\rho = 1.0$ g/cm^3 $P_\rho(T)$ isochores for TIP4P. The $\rho = 0.8$ g/cm^3 and $\rho = 0.9$ g/cm^3 $P_\rho(T)$ isochores for ST2 are also shown for comparison. The TIP4P data indicate that the $\rho = 0.9$ g/cm^3 $P_\rho(T)$ isochore has positive slope between $T = 250$ K and $T = 200$ K. The minimum of the $\rho = 0.9$ g/cm^3 $P_\rho(T)$ TIP4P isochore is therefore expected to occur *below* $T = 200$ K. In contrast, the minimum of the $\rho = 1.0$ g/cm^3 $P_\rho(T)$ TIP4P isochore is clearly above $T = 200$ K. Therefore the TMD line in

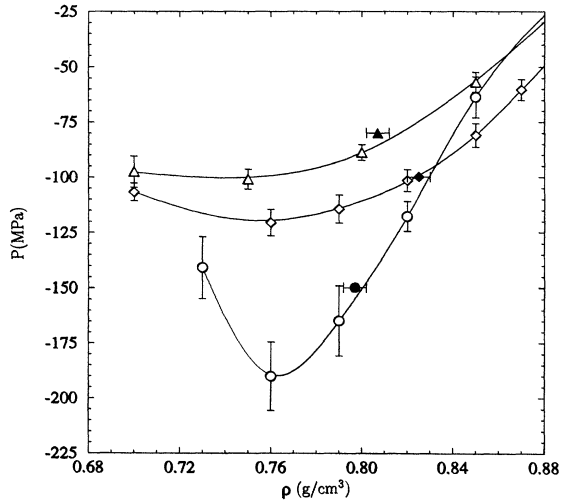

FIG. 4. Detail of the $P_T(\rho)$ isotherms for the $N = 216$ ST2 simulations at $T = 290$ K (○), $T = 330$ K (◇), and $T = 360$ K (△). For each isotherm, the filled symbol shows the result of the $N = 1728$ constant-P ST2 simulation at the same T.

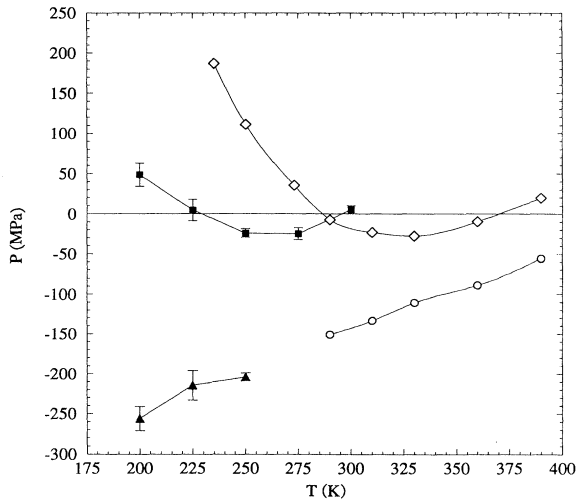

FIG. 5. $P_\rho(T)$ isochores for TIP4P at $\rho = 1.0$ g/cm^3 (filled □) and $\rho = 0.9$ g/cm^3 (filled △), and for ST2 at $\rho = 0.9$ g/cm^3 (◇) and $\rho = 0.8$ g/cm^3 (○).

the TIP4P phase diagram must take on positive slope at sufficiently negative P, as it does in ST2. The behavior of TIP4P is thus shown again to be similar to the ST2 behavior, and *not* consistent with the predictions of the SLC. This check makes less plausible the possibility that the properties observed in the ST2 phase diagram for $P < 0$ are unphysical artifacts associated with the ST2 model.

V. IMPLICATIONS FOR $(\partial U/\partial V)_T$

In this section, we show that the thermodynamic behavior indicated in Fig. 3(b) can also be observed in the relationship between U and V. We begin with the thermodynamic identity

$$\left(\frac{\partial U}{\partial V}\right)_T = T\left(\frac{\partial S}{\partial V}\right)_T - P, \tag{5.1}$$

which follows from $P = -(\partial A/\partial V)_T$ where $A = U - TS$ is the Helmholtz potential. The term $-(\partial U/\partial V)_T$ represents the energetic contribution to the total pressure, while $T(\partial S/\partial V)_T$ is the corresponding entropic contribution. Note that $T(\partial S/\partial V)_T$ is proportional to α_P, using the Maxwell relation $(\partial S/\partial V)_T = (\partial P/\partial T)_V$, and the fact that γ_V is related to α_P through Eq. (1.5). Since K_T is always positive in the stable and metastable region, γ_V will always have the same sign as α_P.

We note that two well-defined behaviors for $(\partial U/\partial V)_T$ can be predicted by Eq. (5.1), and by the knowledge of the sign of α_P.

(i) In the region of positive P and negative α_P, as in real water at atmospheric P below 4 °C, $(\partial U/\partial V)_T$ must be negative. This follows from Eq. (5.1) when $P > 0$, and because $T(\partial S/\partial V)_T < 0$ when $\alpha_P < 0$. Thus, in this region, fluctuations of energy and volume must be anticorrelated [47]. This observation confirms the expectation [48–52] that an increase in local volume strengthens the network of H bonds in the liquid at sufficiently low T.

(ii) Next we note that α_P, and therefore $T(\partial S/\partial V)_T$, is always positive in the vicinity of the spinodal for the phase behavior depicted in Fig. 3(b). The thermodynamic identity Eq. (5.1) then leads to the requirement that $(\partial U/\partial V)_T$ be positive, since $P < 0$ in the vicinity of the spinodal. We can confirm that this is indeed the case in the ST2 data by plotting, in Fig. 6, isotherms of U as a function of V: in all cases where the spinodal is reached, $(\partial U/\partial V)_T > 0$ near the specific volume of the spinodal. A corresponding plot of the TIP4P data for U from Table IV gives the same result.

The nonmonotonic behavior of U in Fig. 6 admits of physical interpretation. At high temperatures where no TMD is observed at any V, U as a function of V always has positive slope, as expected for a normal low-density liquid in which V is increasing. At lower T where the TMD line is observed, a V range emerges where U takes on negative slope. This is an indication that the random H-bond network is enhanced by stretching the liquid at lower temperatures. However, even at these lower temperatures, U again takes on positive slope at sufficiently large V, at the extremes of stretching.

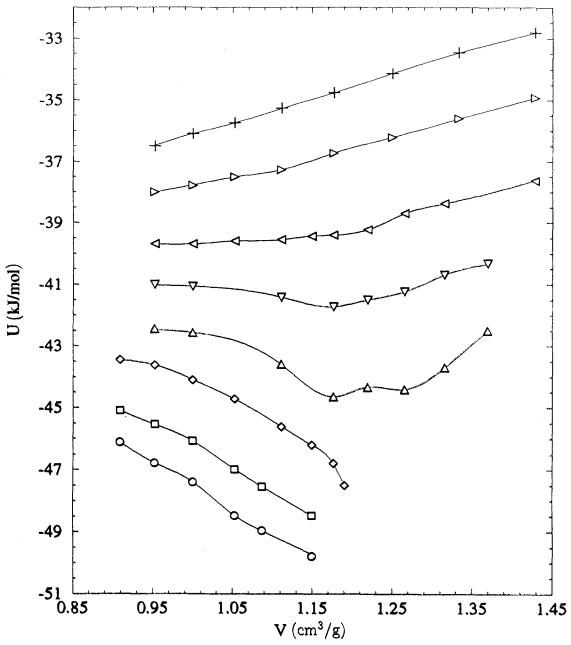

FIG. 6. ST2 isotherms of U vs V at $T = 390$ K (+), $T = 360$ K (▷), $T = 330$ K (◁), $T = 310$ K (▽), $T = 290$ K (△), $T = 273$ K (◇), $T = 250$ K (□), and $T = 235$ K (○). Splines (solid lines) are drawn through each isotherm.

One possible interpretation of this result arises from considering the possible evolution of the molecular structure as the liquid is stretched. U first decreases with V during the initial phase of stretching because the formation of more perfectly formed H bonds is facilitated by the larger volume per molecule becoming available. However, this process can only proceed to a finite extent before V increases so much that even a fully formed four-coordinated open network of H bonds cannot fill the volume being made available. In this regime, the H bonds are for the most part already straight, and stretching can only be accommodated through stretching *along* H bonds. This process necessarily induces U to increase again, and may also cause the entropy S to increase with increasing V in this extreme of stretching, since the increasing molecular volume in this regime ceases to further improve the tetrahedrality of the H-bond network. If this is the case, then in the extremes of stretching, the system ceases to display the anomalous feature that S decreases with an increase in V ($\alpha_P < 0$). Thus this behavior is consistent with the possibility that the vicinity of the spinodal is characterized by $\alpha_P > 0$.

VI. IMPLICATIONS FOR STRUCTURE

An examination of the molecular structure of the stretched liquid can afford insight into the thermo-

dynamic behavior discussed in the preceding section. Specifically, we can verify near the spinodal the suppression of thermodynamic anomalies such as $\alpha_P < 0$ (i.e., a return to more normal liquid behavior). In the preceding section, it was inferred from the behavior of U that, upon initially being stretched, the open network of H bonds becomes better formed as V increases. This process necessarily removes disorder from the network of H bonds since the four-coordinated network has a lower entropy.

We can monitor this tendency toward entropy reduction by examining how the peaks of the three atomic radial distribution functions (RDF's)— $g_{OO}(r)$, $g_{OH}(r)$, and $g_{HH}(r)$—sharpen as V increases, as shown for states of the ST2 liquid along the $T = 290$ K isotherm in Fig. 7(a). A quantitative (though arbitrary) measure of this sharpening is the value of the RDF at its first minimum, which should decrease as the coordination shells become better defined. In Fig. 7(b) are shown isotherms of the value $M_T(\rho)$ of the first minimum of the ST2 oxygen-oxygen RDF as a function of ρ. Consistent with the increasing order in the H-bond network, the value of the minimum initially drops as the system is stretched. However, in all cases where the spinodal is reached, there is a tendency for $M_T(\rho)$ to flatten, and perhaps pass through a minimum as the immediate vicinity of the spinodal is probed. The ordering phenomena seen in the anomalous liquid therefore seem to be reversed in the regime of most extreme stretching, consistent with the possibility that $(\partial S/\partial V)_T > 0$ near the spinodal as inferred from the behavior of U. An analysis of the RDF's resulting from the TIP4P simulations corroborates this result.

The structure of *stretched* liquid water has not been directly measured in experiments because of the difficulties of maintaining the homogeneous liquid under high tension. However, previous simulation studies of stretched water by Geiger and co-workers [53,54] have predicted that the stretched liquid structure tends toward that of a four-coordinated random network. This prediction was justified through a consideration of the structure of the low-density amorphous (LDA) ice, formed via vapor deposition [55,56]. LDA ice has both structural and thermodynamic characteristics that are consistent with its being the amorphous solid realization of a four-coordinated random network of water molecules [55]. Geiger and co-workers showed that the structure of simulated stretched liquid water is very similar to that of LDA ice.

It is useful to reproduce the comparison between stretched water and LDA ice here, since more structural studies of the LDA ice have become available since the original work of Geiger and co-workers. Determinations of the LDA ice structure have been made by Bellissent-Funel *et al.* via neutron scattering [56,57]. In these experiments, the Fourier transform $h(r)$ of the static structure factor $S(q)$ is the most direct real-space representation of the system. The function $h(r)$ is a weighted sum of the atomic RDF's, where the weights are determined by the intensity of the neutron scattering from specific pairs of atomic species. The relative weights are such that $h(r)$ may be expressed for pure water as [55]

$$h(r) = 4\pi\rho r[0.092g_{OO}(r) + 0.422g_{OH}(r) + 0.486g_{HH}(r) - 1]. \quad (6.1)$$

This $h(r)$ function can easily be evaluated from the con-

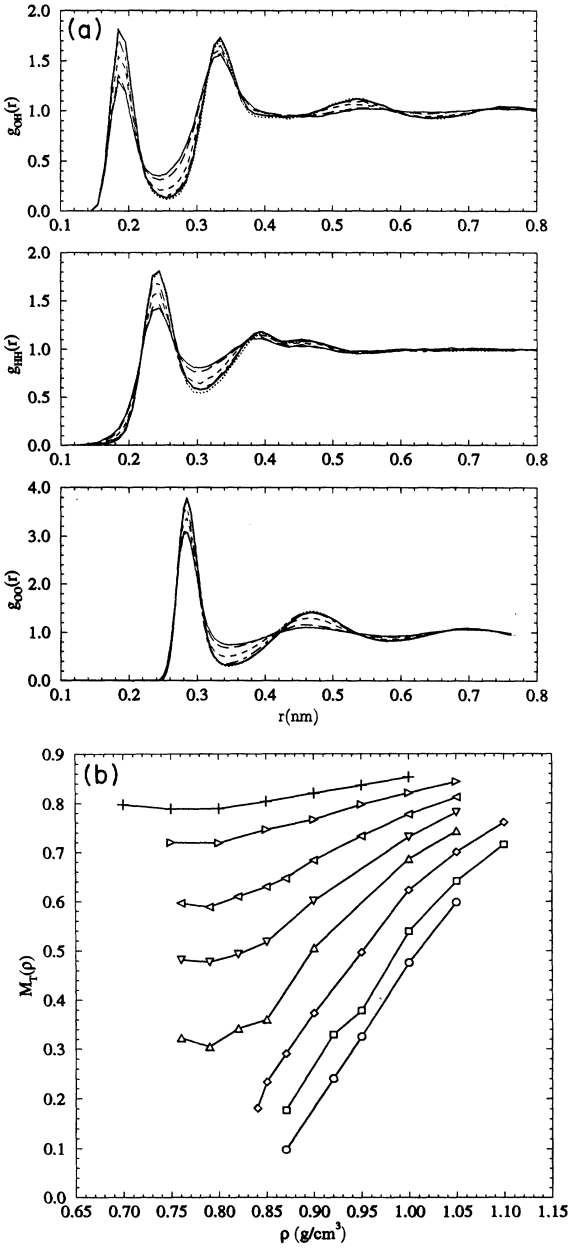

FIG. 7. (a) $g_{OH}(r)$, $g_{HH}(r)$, and $g_{OO}(r)$, for the $T = 290$ K ST2 liquid at $\rho = 1.05$ g/cm^3 (thin line), $\rho = 1.00$ g/cm^3 (long-dashed line), $\rho = 0.90$ g/cm^3 (short-dashed line), $\rho = 0.85$ g/cm^3 (dot-dashed line), $\rho = 0.79$ g/cm^3 (dotted line), and $\rho = 0.76$ g/cm^3 (thick line). (b) Isotherms of $M_T(\rho)$, the first minimum of $g_{OO}(r)$, as a function of ρ at $T = 235$ K ($\circ$), $T = 250$ K ($\square$), $T = 273$ K ($\diamond$), $T = 290$ K ($\triangle$), $T = 310$ K ($\triangledown$), $T = 330$ K ($\triangleleft$), $T = 360$ K ($\triangleright$), and $T = 390$ K ($+$).

figurations resulting from the simulations, and is shown in Fig. 8(a) at several densities of the ST2 system for $T = 290$ K. From the standpoint of $h(r)$, there seems to be a marked evolution in the organization of the system as it is stretched.

Figure 8(b) compares $h(r)$ as determined from experiments on the liquid [56,58] with the simulated ST2 and TIP4P liquids at the same density, and suggests that the simulations approximate the real liquid structure to a fair degree. In Fig. 8(c) the structure of LDA ice [56,58] is compared to that of the simulated stretched liquid for ST2 and TIP4P. The change in liquid structure on stretching does seem to be in the direction of forming the same structure as that found in the LDA ice. This observation in turn confirms the suggestion [53,54] that stretched water is indeed tending toward a four-coordinated random network. The result of the present study is to show that such a stretched liquid may possess a thermodynamic behavior in which anomalies are suppressed by extreme stretching. In fact, it is the very possibility that a four-coordinated random network can form, and then *itself* be stretched, that makes this phenomenon possible.

Note that it is significant that a substance with a similar structure to that of LDA ice can (at least in simulation) be formed *continuously* from the liquid at ambient T via stretching. This observation bears on the question of the thermodynamic relationship between liquid

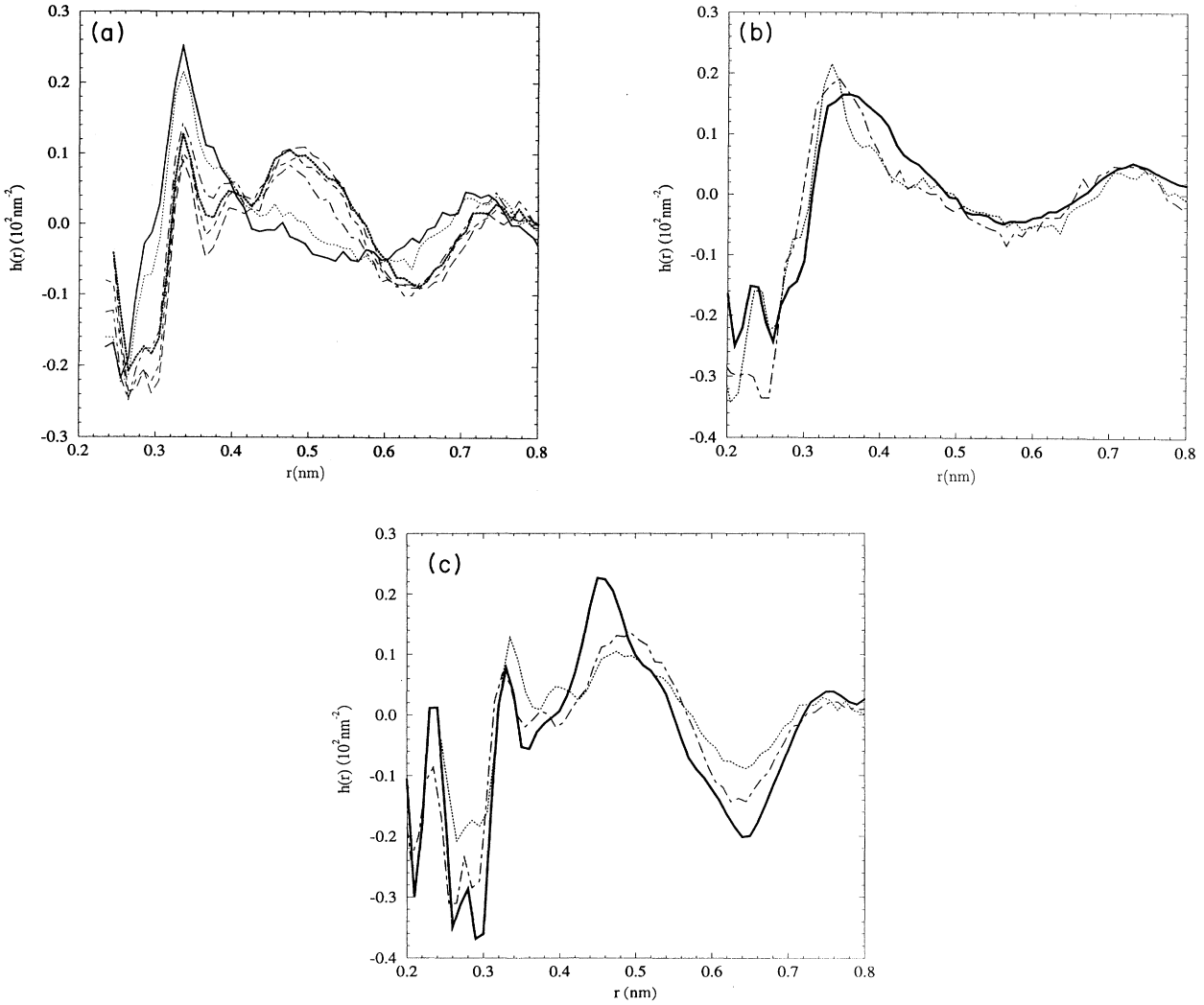

FIG. 8. (a) $h(r)$ of the ST2 liquid at $T = 290$ K at $\rho = 1.05$ g/cm^3 (thick solid line), $\rho = 1.00$ g/cm^3 (dotted line), $\rho = 0.90$ g/cm^3 (dot-dashed line), $\rho = 0.85$ g/cm^3 (short-dashed line), $\rho = 0.79$ g/cm^3 (long-dashed line), and $\rho = 0.76$ g/cm^3 (thick dotted line). (b) $h(r)$ at $\rho = 1.0$ g/cm^3 for ST2 at $T = 290$ K (dotted line), and TIP4P at $T = 300$ K (dot-dashed line), compared to $h(r)$ of liquid D_2O at $T = 284$ K and $\rho = 1.0$ g/cm^3 (solid line) as measured by Bellissent-Funel, *et al.* [56]. (c) $h(r)$ of ST2 at $T = 290$ K, $\rho = 0.76$ g/cm^3, and $P = -190$ MPa (dotted line), and of TIP4P at $T = 225$ K, $\rho = 0.85$ g/cm^3, and $P = -314$ MPa (dot-dashed line), compared to $h(r)$ of low-density amorphous ice (solid line) as measured by Bellissent-Funel *et al.* [56].

water and LDA ice. If the quenched form of this simulated low-density liquid is identified with the LDA ice, then the simulations suggest that there exists a continuous thermodynamic path from the liquid to the LDA ice, at least in a certain regime. The present simulations would therefore be consistent with the possibility that the LDA ice is thermodynamically contiguous with the liquid [59]. However, this view is a subject of ongoing scientific debate [60].

VII. CONCLUSION

The results of this work can be summarized as follows: (1) The spinodal of liquid water as modeled by the ST2 and TIP4P potentials is located and is found not to be reentrant, a result which is not consistent with the predictions of the SLC. (2) The position and shape of the TMD line is also calculated, and it is found to change slope in the metastable region of the phase diagram at $P < 0$. (3) The relationship we find between the spinodal and TMD lines, though not predicted by the SLC, is thermodynamically consistent, and can be incorporated into an understanding of how the energetic and structural properties of the liquid change as it is subjected to tensile stress.

One cannot overstate the fact that our approach cannot *disprove* the existence of a reentrant spinodal in liquid water. The SLC remains a thermodynamically self-consistent possibility. In addition, the predictions of the SLC are similar to those found when the widely used empirical equation of state of Haar *et al.* [39] (which describes thermodynamically stable fluid water) is extrapolated into the metastable region where $P < 0$ [7,20]. Though the thermodynamic behavior derived from extrapolations of a high order polynomial (like that of Haar *et al.*) may give spurious predictions, the SLC itself cannot be similarly dismissed. Our work consists of computer simulations using idealized interparticle potentials (ST2 and TIP4P). Based on our calculations, we propose a different equation of state for water in the region where $P < 0$, which is itself thermodynamically self-consistent. Our present proposal therefore is an alternative to the SLC, but it remains to be determined which applies to real water.

A primary motivation for the SLC is that it provides a means of understanding why a thermodynamic singularity, in the form of a spinodal, could be present in the supercooled region of the phase diagram of liquid water. This singularity would in turn induce the rapid changes in static and dynamic properties observed in experiments on liquid water. A question that therefore remains unanswered in this work is that of the origin of anomalies in liquid water. The present results show that the thermodynamic feature which expresses itself through the anomalies of liquid water may not be a reentrant spinodal. In the absence of a reentrant spinodal, we propose elsewhere [21,43] an alternative thermodynamic feature to explain the anomalies of water.

ACKNOWLEDGMENTS

We thank M. C. Bellissent-Funel, P. Debenedetti, S. C. Glotzer, T. Grande, M. Hemmati, S. Schwarzer, J. Shao, R. J. Speedy, and especially C. A. Angell and S. Sastry, for valuable discussions. Special thanks are also due to L. Striemann and A. Geiger for sharing their preliminary results. Financial support was provided by BP and NSF.

APPENDIX A: INTERACTIONS OF THERMODYNAMIC ANOMALIES AND SPINODALS

This appendix reviews some of the thermodynamic behavior that is possible when a liquid exhibits both a spinodal stability limit and a TMD line. Some of the results below were first demonstrated by Speedy [2] for the specific case of liquid water; the approach given here follows closely the presentation of Debenedetti and co-workers [12–15].

For the purposes of this section, thermodynamic behavior will be discussed in the context of a mean-field approximation in which the spinodal is a well-defined locus of points $P_s(V,T)$. On a $P(V,T)$ EOS surface which itself is everywhere analytic, $P_s(V,T)$ is the locus of points satisfying the condition

$$\left(\frac{\partial P}{\partial V}\right)_T = 0. \tag{A1}$$

In order to determine the properties of the P-T projection of the spinodal line $P_s(T)$, consider the differential dP of P, which is everywhere on $P(V,T)$ equal to

$$dP = \left(\frac{\partial P}{\partial T}\right)_V dT + \left(\frac{\partial P}{\partial V}\right)_T dV. \tag{A2}$$

Along an arbitrary path x embedded in the $P(V,T)$ surface the total derivative of P with respect to T anywhere along x is given by

$$\left(\frac{dP}{dT}\right)_x = \left(\frac{\partial P}{\partial T}\right)_V + \left(\frac{\partial P}{\partial V}\right)_T \left(\frac{\partial V}{\partial T}\right)_x. \tag{A3}$$

Taking the path x to be the spinodal line, Eqs. (A1) and (A3) give the condition

$$\frac{dP_s(T)}{dT} = \left(\frac{\partial P}{\partial T}\right)_V. \tag{A4}$$

The above relation, due to Skripov [61], is significant because it shows that the spinodal line $P_s(T)$ is everywhere tangent to the P-T projection of a $P_\rho(T)$ isochore of the system. In a classical van der Waals liquid-gas system, the liquid spinodal represents the lowest P at which the metastable liquid is observable at a given T. Beyond the liquid spinodal, in the unstable regime, P rises above $P_s(T)$ at fixed T, as shown in Fig. 1(c). Hence, the P-T projection of the liquid spinodal $P_s(T)$ will be a low-P

envelope of the family of metastable liquid isochores, each touching $P_s(T)$ tangentially.

If the system considered also exhibits a density anomaly, the location of a TMD line in the phase diagram is given by the locus of points for which $\alpha_P = 0$, or equivalently, as the locus of $P_\rho(T)$ isochore minima where the condition

$$\left(\frac{\partial P}{\partial T}\right)_V = 0 \tag{A5}$$

is satisfied. Given that both the spinodal and TMD lines can therefore be related to the behavior of $P_\rho(T)$ isochores, it is reasonable to expect that their properties are not independent when they occur in the same phase diagram. This can be seen immediately for the case of an intersection of a TMD and spinodal line: At a TMD-spinodal intersection point R, both Eqs. (A4) and (A5) must be satisfied, with the result that $dP_s(T)/dT = 0$ at R. Also, from Eq. (A4), the sign of $dP_s(T)/dT$ necessarily changes from one side of R to the other, since R is a point where $(\partial P/\partial T)_V$ changes sign. Therefore an extremum occurs in $P_s(T)$ at R.

As stated above, the detailed analysis of the specific thermodynamic constraints on the relationship between the spinodal line and the TMD line was first made by Speedy for the specific case of liquid water, and later by Debenedetti and co-workers for arbitrary fluids exhibiting TMD lines. Their analysis follows from the assumption of the analyticity of the $P(V,T)$ surface, as described above, and provides two main results.

(i) A TMD line cannot end in a thermodynamically self-consistent way without either (a) meeting a line of density *minima* in the $P(V,T)$ surface (a circumstance that has never been experimentally observed), or (b) meeting a spinodal line.

(ii) Only a subset of all conceivable TMD-spinodal line intersections satisfying Eq. (A4) are thermodynamically possible.

In both cases, (i) and (ii) are arrived at by examining the behavior of a truncated Taylor expansion of the $P(V,T)$ surface around a TMD line end point, which is either within the stable or metastable region [yielding (i)], or at the spinodal boundary of the metastable region [yielding (ii)]. The proof of (i), although straightforward, is not particularly important to the conclusions that will be drawn in the present work, and is not reproduced here. However, the method used to obtain (ii), by which a given kind of TMD-spinodal line intersection is assessed for thermodynamic consistency, is useful in the present context, and so is given below.

As shown above, the intersection point R of a spinodal and TMD line is necessarily an extremum of the P-T projection of the spinodal line $P_s(T)$. Therefore, begin by assuming that such an analytic spinodal extremum R exists at (P_R, V_R, T_R), and that a TMD line intersects the spinodal at R. Change coordinates such that the spinodal extremum occurs at the origin, via the transformation:

$$p \equiv P - P_R, \tag{A6}$$

$$v \equiv V - V_R, \tag{A7}$$

and

$$t \equiv T - T_R. \tag{A8}$$

In these variables, everywhere along the spinodal,

$$\left(\frac{\partial p}{\partial v}\right)_t = 0, \tag{A9}$$

while specifically at R, the condition

$$\left(\frac{\partial p}{\partial t}\right)_v = 0 \tag{A10}$$

also holds, since the TMD line intersects the spinodal at R.

Given the analyticity of the $p(v,t)$ surface, expand $p(v,t)$ around R in a Taylor series truncated at second order:

$$p(v,t) = \left(\frac{\partial p}{\partial t}\right)_v t + \left(\frac{\partial p}{\partial v}\right)_t v + \frac{1}{2}\left(\frac{\partial^2 p}{\partial t^2}\right)_v t^2 + \frac{1}{2}\left(\frac{\partial^2 p}{\partial v^2}\right)_t v^2 + \left(\frac{\partial^2 p}{\partial t \partial v}\right) tv. \tag{A11}$$

From Eqs. (A9) and (A10), the linear terms are both zero at R, giving

$$p(v,t) = at^2 + bv^2 + ctv, \tag{A12}$$

where

$$a = \frac{1}{2}\left(\frac{\partial^2 p}{\partial t^2}\right)_v, \tag{A13}$$

$$b = \frac{1}{2}\left(\frac{\partial^2 p}{\partial v^2}\right)_t, \tag{A14}$$

and

$$c = \left(\frac{\partial^2 p}{\partial t \partial v}\right). \tag{A15}$$

The signs of the constants a, b, and c depend on the circumstances being considered. In general, for R to be the intersection of a spinodal with a TMD line [which is a locus of $P_\rho(T)$ isochore minima], isochores in the immediate vicinity of R must have extrema with positive curvature, and given the form of Eq. (A12), this requires $a > 0$. (The constraint $a < 0$ would imply an intersection with a line of density *minima*.) In addition, if R occurs on a liquid spinodal connected to a liquid-gas critical point, then the spinodal necessarily lies below a coexistence line in the p-t plane. In these circumstances, the spinodal represents the first minima along isotherms of p with respect to v; this condition gives $b > 0$. Further, assume that K_T only decreases along an isochore as t increases. This last assumption corresponds to a metastable liquid which never loses mechanical stability on isochoric heating, a condition met by all known liquids; for example, it is easily shown to be true for the van der Waals equation. This last condition requires that $c < 0$, since c indicates the t dependence of $(\partial p/\partial v)_t$, which should only become

more negative as t increases if K_T is to decrease as t increases.

The spinodal $p_s(t)$ in the region of R is easily found as the locus of points on $p(v,t)$ satisfying Eq. (A9). This locus is given by

$$p_s(t) = a(1 - c^2/4ab)t^2. \tag{A16}$$

Similarly, the TMD line is the locus of points on the surface described by Eq. (A12) which satisfy Eq. (A10). The TMD line is thus described by

$$p_{\mathrm{TMD}}(t) = a(4ab/c^2 - 1)t^2. \tag{A17}$$

Now, consider the specific case in which the extremum R is a *minimum* along the spinodal line. (This is the case which is relevant to the prediction for the shape of the spinodal given in the SLC.) From Eq. (A16), it can be seen that for R to occur at a spinodal minimum, the relative magnitudes of a, b, and c must be such that $(1 - c^2/4ab) > 0$, or

$$c^2/4ab < 1. \tag{A18}$$

A plot of the relevant thermodynamic features near R resulting from these conditions is given in Fig. 9. As assumed, the spinodal passes through a minimum and the TMD line intersects it so as to satisfy Eq. (A4). It is particularly important to note that the TMD line does not appear beyond the intersection with the spinodal, in the region where $t > 0$. This can be understood by applying the stability criterion $(\partial p/\partial v)_t < 0$ to points along $p_{\mathrm{TMD}}(t)$: Eq. (A12) gives

$$\left(\frac{\partial p}{\partial v}\right)_t = 2bv + ct. \tag{A19}$$

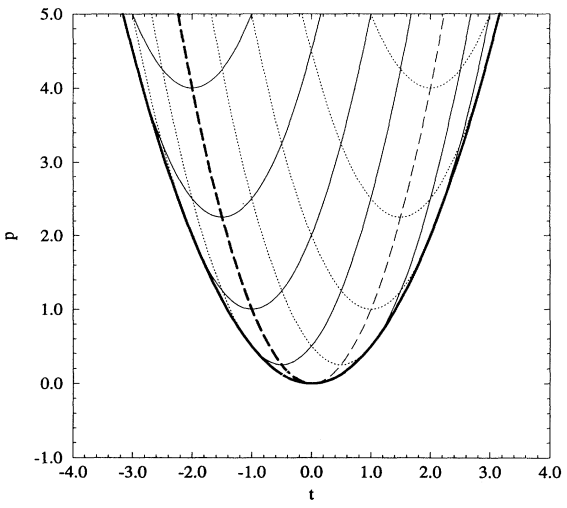

FIG. 9. Intersection of TMD line (heavy dashed line) with spinodal minimum (heavy solid line), as described in Appendix A. $p_v(t)$ isochores of the metastable liquid (thin solid lines) and their extension into the unstable region (dotted lines) are also shown. Note that the stable branch of the TMD line (thick dashed line) only occurs for $t < 0$; its unstable extension at $t > 0$ (thin dashed line) is also shown.

The volume $v_{\mathrm{TMD}}(t)$ of the TMD line is described by

$$v_{\mathrm{TMD}}(t) = (-2a/c)t. \tag{A20}$$

Combining Eqs. (A19) and (A20) gives the expression for $(\partial p/\partial v)_t$ along the TMD line:

$$\left[\left(\frac{\partial p}{\partial v}\right)_t\right]_{\mathrm{TMD}} = c(1 - 4ab/c^2)t. \tag{A21}$$

From Eq. (A18) it must be that $(1 - 4ab/c^2) < 0$. Given that $c < 0$, then only the portion of the TMD line for which $t < 0$ is stable. In this case therefore, the observable TMD line has negative slope and appears only in the $t < 0$ range where $p_s(t)$ also has negative slope. Note that, under the assumptions of this section, the TMD line cannot meet a spinodal minimum with positive slope.

APPENDIX B: SIMULATION PROTOCOL AND RESULTS

The conclusions of this study are based on the results of molecular-dynamics computer simulations of systems of water molecules interacting via a model potential [62]. In this work, the ST2, TIP4P, and SPC/E potentials are all used to varying degrees. Each of these potentials models a single water molecule as a rigid set of interaction sites. Specific sites on different molecules interact via either Lennard-Jones or Coulomb potentials. The total interaction of a given molecule i with another molecule j is calculated explicitly when the separation of the O atom sites on each molecule r_{ij} is less than a cutoff distance r_c. In all cases, we choose $r_c = 2.5\sigma$, where σ is the characteristic length associated with the Lennard-Jones interaction between molecules. The contribution to the force on i due to Coulomb interactions with j when $r_{ij} > r_c$ is approximated using the reaction-field method, as described by Steinhauser [63]. Also, the approximate influence of Lennard-Jones interactions between molecules separated by more than r_c is included in the evaluation of thermodynamic properties like the potential energy U and the pressure P.

Except where otherwise indicated, each simulation is conducted at constant V, with $N = 216$ molecules enclosed in a cubic box having sides of length L chosen so as to give the desired density. Periodic boundary conditions are used throughout. The time step δt for the integration of the molecular trajectories is fixed for all the ST2 simulations at 1 fs. The TIP4P simulations are carried out with either $\delta t = 1$ fs or 2 fs, as indicated in Table IV. The very first simulations were started from configurations of particles distributed throughout the simulation box so that their centers of mass formed a simple cubic lattice, while their initial orientations were chosen at random. After the completion of several such runs, a simulation for a new state point would be started from the final configuration resulting from a simulation of a nearby state point. Equilibration is considered complete when the values of P and U are observed to be clearly fluctuating around a fixed value, and when the rms distance

traversed by the molecules from their starting positions has exceeded *at least* one molecular diameter, taken to be σ.

During both the equilibration phase, and the evaluation of thermodynamic averages following equilibration, the temperature of each simulation is controlled using Berendsen's method of velocity rescaling [64], with a time constant of $\tau_T = 0.5$ ps. Though the use of Berendsen's method does not generate states in either the (N,V,T) or (N,V,E) ensembles, the calculation of the average of P or U is not affected.

In all cases, the total simulation time t_f (that is, equilibration plus post-equilibration) is at least 200 ps except at the highest T. At the lowest V and T simulated, run times of 600 to 800 ps are typical. P and U are calculated as the arithmetic average of the time series of values calculated over the second half of the system trajectory, of length $t_h = t_f/2$ (i.e., the simulation of each state is always run for *at least* enough steps so that the equilibration criteria have been met before the simulation is half complete). The method of calculation of the error in measurements of P and U, respectively δP and δU, is described in Appendix C. The properties of the states simulated are given in Tables II, III, and IV.

To measure structural and dynamic properties, the molecular trajectories resulting from the above procedure are continued in constant-(N,V,E) simulations. From these constant-(N,V,E) runs, the radial distribution functions are calculated from the particle positions, and the diffusion constant D is calculated from the mean square displacement of the particles as a function of time. These constant-(N,V,E) simulations also confirm that the values of P and U measured when T is constrained via Berendsen's method reproduce the values that are calculated from simulations in the (N,V,E) ensemble.

APPENDIX C: METHOD FOR ESTIMATION OF ERROR IN MEASUREMENTS OF THERMODYNAMIC PROPERTIES

This section describes the method used to evaluate the error δP in the estimations of the average pressure P quoted in Tables II, III, and IV. In all cases, P is estimated from the second half of the total simulation history. Denote the average over 1 ps (1000 time steps when $\delta t = 1$ fs) of the instantaneous pressure calculated at each time step, by P_1. The time series of P_1 for the ST2 simulations at $\rho = 1.0$ g/cm^3 for several different T are shown in Fig. 10(a). The fluctuations observed in these time series over the second half of the system trajectory represent the error δP_1 observed when P is estimated from any single 1 ps segment of the simulation. If the decay time τ for correlations in these time series can be estimated, then the number N_h of *independent* estimates of P available from the time series of P_1 is just $N_h = t_h/\tau$. If the fluctuation δP_1 is calculated as

$$\delta P_1 = \left(\frac{1}{t_h} \sum_{t=t_h}^{t_f} [P_1(t) - P]^2 \right)^{1/2}, \tag{C1}$$

then δP is just

$$\delta P = \frac{\delta P_1}{N_h^{1/2}}. \tag{C2}$$

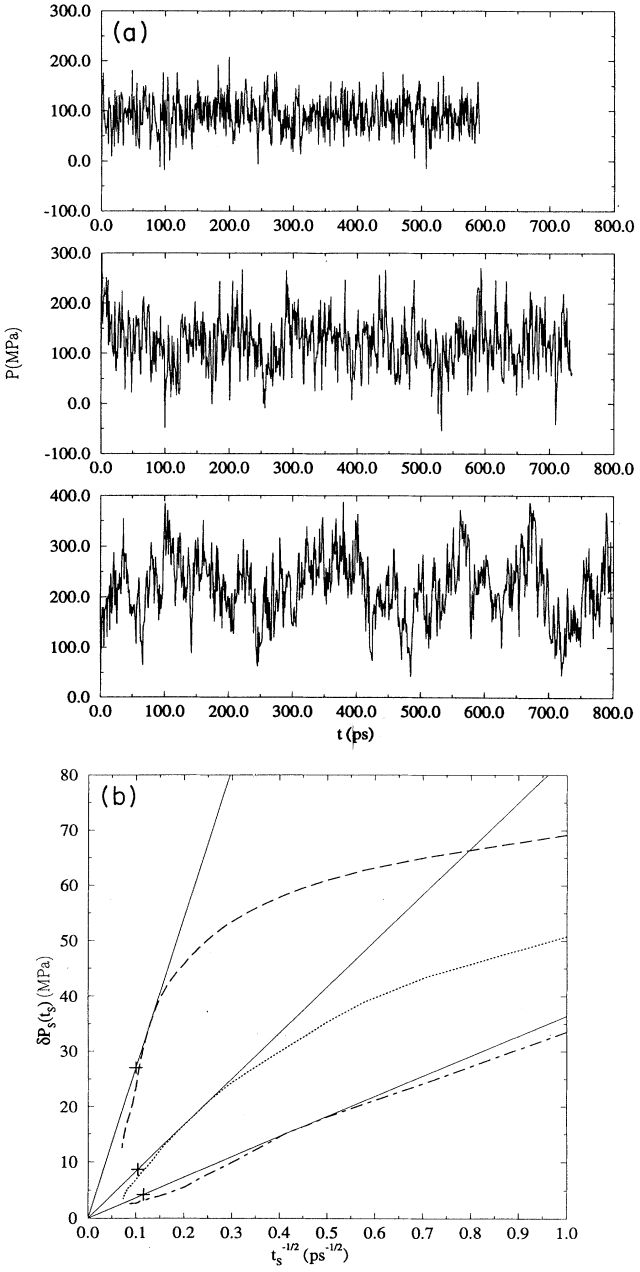

FIG. 10. (a) Time series of P_1 for ST2 over the total time of simulation at $\rho = 1.0$ g/cm^3, for $T = 330$ K (top), $T = 273$ K (middle), and $T = 235$ K (bottom). (b) Dependence of δP_S on $t_S^{-1/2}$, for $T = 330$ K (dot-dashed line), $T = 273$ K (dotted line), and $T = 235$ K (dashed line). For each curve, the accompanying solid line passes through the origin and touches the curve tangentially from above; the crosses indicate the points on the straight lines taken to give the values of δP cited in Appendix B.

An estimate of τ is available from a plot of the autocorrelation function $C(t)$ of the time series of P_1, defined as

$$C(t) = \frac{\langle P_1(t_0)P_1(t_0+t)\rangle - \langle P_1\rangle^2}{\langle P_1^2\rangle - \langle P_1\rangle^2}, \qquad \text{(C3)}$$

where $\langle P_1(t_0)P_1(t_0+t)\rangle$ is an average over all possible starting times t_0, and $\langle P_1\rangle = P$ and $\langle P_1^2\rangle$ are both averages taken over the second half of the time series. The order of magnitude of τ can be estimated as the time at which $C(t)$ begins fluctuating about zero. As expected from the form of the time series, the corresponding $C(t)$ functions show that τ is increasing at lower T, and is certainly many tens of picoseconds at $T = 273$ K. However, in general the $C(t)$ plots are found to be very noisy, making accurate estimation of τ (for example, via fitting to an exponential form) difficult.

As an alternative to evaluating δP through an estimate of τ, the following approach is possible: Consider the second half of the simulation (of length t_h) from which P is obtained. Divide this full interval into S segments each of length $t_S = t_h/S$. If the average of P_1 within each segment is denoted P_S, then the fluctuation δP_S of P_S over all S segments is

$$\delta P_S = \left\langle \left(\frac{1}{S} \sum_{i=1}^{S} [P_S(i) - P]^2 \right)^{1/2} \right\rangle, \qquad \text{(C4)}$$

where here i labels the S different segments, and where the average $\langle\,\rangle$ is the average over all possible different ways of dividing the second half of the simulation into S segments. Although the statistics become poor for the calculation of δP_S as $t_S \to t_h$, since this means that $S \to 1$, the trend in δP_S as a function of t_S contains useful information. Specifically, if $t_S > \tau$, then δP_S should be a linearly increasing function of $t_S^{-1/2}$ which passes through the origin. Figure 10(b) shows the dependence of δP_S on $t_S^{-1/2}$ for the time series given in Figure 10(a). Figure 10(b) thus indicates the decay of the error in the estimation of P as a larger and larger piece of the simulation is used in the average. Figure 10(b) confirms the prediction that, once t_S becomes greater than τ, δP_S becomes a linear function of $t_S^{-1/2}$.

To complete the act of estimating δP, an upper bound on the behavior of δP_S as it approaches $t_S^{-1/2} = 0$ is taken as a straight line passing through the origin which tangentially touches the δP_S curve from above, as shown in Fig. 10(b). The value of δP_S along this straight line at $t_S^{-1/2} = t_h^{-1/2}$ estimates the error δP in the value of P made using the entire second half of the simulation. In order to ensure a conservative estimate of δP, the error quoted in Tables II, III, and IV is actually twice this value. In other words, the error δP in Tables II, III, and IV represents the error in an estimation of P in which the average is taken over a time slice of size $t_h/4$; this time and error for each time series is indicated by the + signs in Fig. 10(b). Although this approach doubles the error which might justifiably be quoted, it ensures that the error given is consistent with the variation in estimates of P actually calculated from subsegments of the simulation. Note also that the error δU in the average potential energy U is evaluated in exactly the same way.

[1] R. J. Speedy and C. A. Angell, J. Chem. Phys. **65**, 851 (1976).
[2] R. J. Speedy, J. Phys. Chem. **86**, 982 (1982).
[3] R. J. Speedy, J. Phys. Chem. **86**, 3002 (1982).
[4] R. J. Speedy, J. Phys. Chem. **91**, 3354 (1987).
[5] C.A. Angell, in *Water: A Comprehensive Treatise*, edited by F. Franks (Plenum Press, New York, 1981), Vol. 7, p. 1.
[6] E.W. Lang and H.-D. Lüdemann, Angew. Chem. Int. Ed. Engl. **21**, 315 (1982).
[7] C.A. Angell, Annu. Rev. Phys. Chem. **34**, 593 (1983).
[8] F. X. Prielmeier, E. W. Lang, R. J. Speedy, and H.-D. Lüdemann, Phys. Rev. Lett. **59**, 1128 (1987).
[9] F. X. Prielmeier, E. W. Lang, R. J. Speedy, and H.-D. Lüdemann, Ber. Bunsenges. Phys. Chem. **92**, 1111 (1988).
[10] C.A. Angell and H. Kanno, Science **193**, 1121 (1976).
[11] S. J. Henderson and R. J. Speedy, J. Phys. Chem. **91**, 3062 (1987).
[12] P. G. Debenedetti and M. C. D'Antonio, J. Chem. Phys. **84**, 3339 (1986).
[13] P. G. Debenedetti and M. C. D'Antonio, J. Chem. Phys. **85**, 4005 (1986).
[14] M. C. D'Antonio and P. G. Debenedetti, J. Chem. Phys. **86**, 2229 (1987).
[15] P. G. Debenedetti and M. C. D'Antonio, AIChE J. **34**, 447 (1988).
[16] P. G. Debenedetti, V. S. Raghavan, and S. S. Borick, J. Phys. Chem. **95**, 4540 (1991).
[17] S. Sastry, F. Sciortino and and H. E. Stanley, J. Chem. Phys. **98**, 9863 (1993); Chem. Phys. Lett. **207**, 275 (1993).
[18] S. J. Henderson and R. J. Speedy, J. Phys. Chem. **91**, 3069 (1987).
[19] J. L. Green, D. J. Durben, G. H. Wolf, and C. A. Angell, Science **249**, R649 (1990).
[20] Q. Zheng, D. J. Durben, G. H. Wolf, and C. A. Angell, Science **254**, R829 (1991).
[21] P. H. Poole, F. Sciortino, U. Essmann, and H. E. Stanley, Nature (London) **360**, 324 (1992).
[22] F. H. Stillinger and A. Rahman, J. Chem. Phys. **60**, 1545 (1974).
[23] W. L. Jorgensen, J. Chandrasekhar, J. Madura, R. W. Impey, and M. Klein, J. Chem. Phys. **79**, 926 (1983).
[24] J.D. Gunton, M. San Miguel, and P.S. Sahni, in *Phase Transitions and Critical Phenomena*, edited by C. Domb and J.L. Lebowitz (Academic Press, London, 1983), Vol. 8, p. 267.
[25] H.E. Stanley, *Introduction to Phase Transitions and Critical Phenomena* (Oxford University Press, Oxford, 1971).

[26] A. Compagner, Physica **72**, 115 (1974).
[27] C. A. Angell, J. Shuppert, and J. C. Tucker, J. Phys. Chem. **77**, 3092 (1973).
[28] For some quantities, in order to fit successfully to a power-law form, it is first necessary to divide the quantity into a sum of "normal" and "singular" parts, and to associate the singular part with X in Eq. (1.2).
[29] H. Kanno and C.A. Angell, J. Chem. Phys. **70**, 4008 (1979).
[30] H. Kanno, R.J. Speedy, and C.A. Angell, Science **189**, 880 (1975).
[31] K. Okasaki, S. Nose, Y. Kataoka, and T. Yamamoto, J. Chem. Phys. **75**, 5864 (1981).
[32] Y. Kataoka, H. Hamada, S. Nose, and T. Yamamoto, J. Chem. Phys. **77**, 5699 (1982).
[33] Y. Kataoka, Bull. Chem. Soc. Jpn. **57**, 1522 (1984).
[34] Y. Kataoka, Bull. Chem. Soc. Jpn. **59**, 1425 (1986).
[35] Y. Kataoka, J. Chem. Phys. **87**, 589 (1987).
[36] L. Striemann, Ph.D. thesis, Universität Dortmund, 1992 (unpublished).
[37] H. J. C. Berendsen, J. R. Grigera, and T. P. Straatsma, J. Phys. Chem. **91**, 6269 (1987).
[38] J. L. Finney, J. E. Quinn, and J. O. Baum, in *Water Science Reviews 1,* edited by F. Franks (Cambridge University Press, Cambridge, England, 1985), and references therein.
[39] L. Haar, J.S. Gallagher, and G. Kell, *NBS/NRC Steam Tables* (Hemisphere Publishing, Washington, 1985).
[40] T. A. Weber and F. H. Stillinger, J. Chem. Phys. **80**, 483 (1984).
[41] Isotherms at lower temperatures do not display minima since the decrease in mobility as T decreases prevents equilibration in reasonable computation times.
[42] W.H. Press, B.P. Flannery, S.A. Teukolsky, and W.T. Vetterling, *Numerical Recipes* (Cambridge University Press, Cambridge, England, 1988).
[43] P. H. Poole, Ph.D. thesis, Boston University, 1993 (unpublished). Available through University Microfilms International, Ann Arbor, Michigan.
[44] The method of Berendsen *et al.* [64] is used (with a time constant of $\tau_P = 0.5$ ps) to constrain P near a desired value. In each case, the desired P is set equal to the average P calculated during the prior constant-V simulations.
[45] F. H. Stillinger and T. A. Weber, J. Chem. Phys. **68**, 3837 (1978).
[46] The simulation scheme is, except for the larger system size, identical to that employed in the $N = 216$ simulation. Each system evolves for 50 ps starting from a cubic lattice initial configuration with randomized orientations. After this first stage of equilibration, the simulations are continued, but now both T and P are controlled with the Berendsen method [64], thus allowing ρ to fluctuate. The fixed value of P was chosen to be the average P in the second half of the initial 50 ps constant-V stage.
[47] G. Ruocco, M. Sampoli, and R. Vallauri, J. Chem. Phys. **96**, 6167 (1992). Note that these authors find only a *positive* correlation between fluctuations of energy and volume in their study of a system of TIP4P molecules. This observation is possible because their system was simulated at T greater than that of the TMD line for TIP4P, where $\alpha_P > 0$
[48] H.E. Stanley and J. Teixeira, J. Chem. Phys. **73**, 3404 (1980).
[49] H. E. Stanley, J. Teixeira, A. Geiger, and R. L. Blumberg, Physica A **106**, 260 (1981).
[50] R. L. Blumberg, H. E. Stanley, A. Geiger, and P. Mausbach, J. Chem. Phys. **80**, 5230 (1984).
[51] A. Geiger and H. E. Stanley, Phys. Rev. Lett. **49**, 1749 (1982).
[52] F. Sciortino, A. Geiger, and H. E. Stanley, Nature (London) **354**, 218 (1991); J. Chem. Phys. **96**, 3857 (1992).
[53] A. Geiger, P. Mausbach, and J. Schnitker, in *Water and Aqueous Solutions*, edited by G. W. Neilson and J. E. Enderby (Adam Hilger, Bristol, 1986), pp. 15–30.
[54] P. Mausbach and A. Geiger, Abschlußbericht des Forschungsprojekts Az. I/60036 der Stiftung Volkswagenwerk, Aachen, 1986 (unpublished).
[55] M. R. Chowdhury, J. C. Dore, and J. T. Wenzel, J. Non-Cryst. Sol. **53**, 247 (1982).
[56] M.-C. Bellissent–Funel, J. Teixeira, and L. Bosio, J. Chem. Phys. **87**, 2231 (1987). In this case, the LDA ice is the substance formed by heating above 128 K the high-density amorphous ice formed via pressure-induced amorphization of ice I_h.
[57] M.-C. Bellissent-Funel, L. Bosio, A. Hallbrucker, E. Mayer, and R. Sridi-Dorbez, J. Chem. Phys. **97**, 1282 (1992).
[58] A. Bizid, L. Bosio, A. Defrain, and M. Oumezzine, J. Chem. Phys. **87**, 2225 (1987).
[59] A similar observation was made in a supercooling experiment by Bellissent-Funel, *et al.*, J. Phys. Condens. Matter **1**, 7123 (1989). On supercooling liquid water at ambient pressure it was found that the structure evolved towards that of the LDA ice.
[60] R. J. Speedy, J. Phys. Chem. **96**, 2322 (1992).
[61] V.P. Skripov, Teplofiz. Vys. Temp. **4**, 816 (1966); High Temp. **4**, 757 (1966).
[62] M.P. Allen and D.J. Tildesley, *Computer Simulation of Liquids* (Oxford University Press, Oxford, 1989).
[63] O. Steinhauser, Mol. Phys. **45**, 335 (1982).
[64] H. J. C. Berendsen, J. P. M. Postma, W. F. van Gunsteren, A. DiNola, and J. R. Haak, J. Chem. Phys. **81**, 3684 (1984).